Power Line Communications over Time-Varying Frequency-Selective Power Line Channels for Smart Home Applications

Thesis submitted in accordance with the requirements of
the University of Liverpool for the degree of Master in Philosophy

By
Wenfei Zhu

July 2014

Abstract

Many countries in the world are developing the next generation power grid, the smart grid, to combat the ongoing severe environmental problems and achieve efficient use of the electricity power grid. Smart metering is an enabling technology in the smart grid to address the energy wasting problem. It monitors and optimises the power consumption of consumers' devices and appliances. To ensure proper operation of smart metering, a reliable communication infrastructure plays a crucial role.

Power line communication (PLC) is regarded as a promising candidate that will fulfil the requirements of smart grid applications. It is also the only wired technology which has a deployment cost comparable to wireless communication. PLC is most commonly used in the low-voltage (LV) power network which includes indoor power networks and the outdoor LV distribution networks. In this thesis we consider using PLC in the indoor power network to support the communication between the smart meter and a variety of appliances that are connected to the network.

Power line communication (PLC) system design in indoor power network is challenging due to a variety of channel impairments, such as time-varying frequency-selective channel and complex impulsive noise scenarios. Among these impairments, the time-varying channel behaviour is an interesting topic that hasn't been thoroughly investigated. Therefore, in this thesis we focus on investigating this behaviour and developing a low-cost but reliable PLC system that is able to support smart metering applications in indoor environments.

To aid the study and design of such a system, the characterisation and modelling of indoor power line channel are extensively investigated in this thesis. In addition, a flexible simulation tool that is able to generate random time-varying indoor power line channel realisations is demonstrated.

Orthogonal frequency division modulation (OFDM) is commonly used in existing PLC standards. However, when it is adopted for time-varying power line channels, it may experience significant intercarrier interference (ICI) due to the Doppler spreading caused by channel time variation. Our investigation on the performance of an ordinary OFDM system over time-varying power line channel reveals that if ICI is not properly compensated, the system may suffer from severe performance loss. We also investigate the performance of some linear equalisers including zero forcing (ZF), minimum mean

squared error (MMSE) and banded equalisers. Among them, banded equalisers provide the best tradeoff between complexity and performance.

For a better tradeoff between complexity and performance, time-domain receiver windowing is usually applied together with banded equalisers. This subject has been well investigated for wireless communication, but not for PLC. In this thesis, we investigate the performance of some well-known receiver window design criteria that was developed for wireless communication for time-varying power line channels. It is found that these criteria do not work well over time-varying power line channels. Therefore, to fill this gap, we propose an alternative window design criterion in this thesis. Simulations have shown that our proposal outperforms the other criteria.

Acknowledgement

I would like to express my sincere gratitude to my supervisor Dr. Xu Zhu for her kindly help and patient guidance throughout this research. Without her constructive advice, encouragement and support, this thesis could not be finished.

I would like to thank my supervisor Prof. Eng Gee Lim for his valuable suggestions on my research work and his great support on my research life at Xi'an Jiaotong-Liverpool University.

I would like to thank my supervisor Prof. Yi Huang for giving me valuable guidance and advice on my research work.

I would like to thank Xi'an Jiaotong-Liverpool University for her financial support of my research.

I would also like to thank my friends and colleagues who have offered kindly suggestions and encouragement during my study.

This thesis is dedicated to my parents and my ex-wife for their greatest support and deepest love all the time.

Contents

List of Figures

List of Tables

Acronyms

2TL two-conductor transmission line. 2, 3, 14, 16, 17, 22, 26, 36, 61

3G the third generation of mobile telecommunications technology. 6, 7

4G the fourth generation of mobile telecommunications technology. 6, 7

AC alternating current. 25, 28, 30, 35, 45

AMI automatic metering infrastructure. 5

AWGN additive white Gaussian noise. 40, 62

BAE band approximation error. vi, vii, ix, x, 11, 49–55, 57–59, 62–64, 66

BB broadband. 8, 9

BER bit error rate. vii, ix, x, 2, 39, 44, 45, 47, 48, 54, 58–60

CENELEC European Committee for Electrotechnical Standardization. 9

CP cyclic prefix. ix, 10, 39, 40, 45, 50

DFT discrete Fourier transform. 39, 40, 42, 43, 50, 53

EM electromagnetic. 16, 17, 28

FFT fast Fourier transform. 50

HAN home area network. ix, 6–9, 61

HDR high data rate. 8, 9

HEMS home energy management system. 5

HV high-voltage. 6

ICI intercarrier interference. i, v, vi, 2, 3, 9–11, 31, 39, 41–45, 47, 57, 61

IEEE Institute of Electrical and Electronics Engineers. 8, 39

IFFT inverse fast Fourier transform. 39

IONR in-band signal to out-of-band interference noise ratio. vi, vii, 50–55, 59, 62, 65, 66

ISI inter-symbol interference. 10, 40

ITU-T International Telecommunication Union Telecommunication Standardization Sector. 8, 39

LDR low data rate. 8, 9

LPTV linear periodic time-varying. ix, 26, 29, 31, 32, 36

LS least square. 43

LTI linear time-invariant. 10, 42

LTV linear time-variant. ix, 39, 41, 43

LV low-voltage. i, 6, 7, 15

MIMO multiple-input-multiple-output. 22, 62

ML maximum likelihood. 11, 39

MMSE minimum mean squared error. i, ii, 10, 43–47, 50, 53, 59

MSE mean squared error. 50

MTL multi-conductor transmission line. 2, 3, 14, 17, 19, 22, 36, 61, 62

MV medium-voltage. 6, 7, 15

NAN neighbourhood area network. 6, 7

NB narrowband. 8–10, 33, 39, 45

OFDM orthogonal frequency division modulation. i, v, vi, ix, 2, 3, 6, 9, 10, 31, 32, 37, 39, 40, 42, 43, 45, 46, 50, 53, 58

OOB out-of-band. 43, 45, 47, 49, 51, 52, 55–57

OPERA Open PLC European Research Alliance. ix, 15

p.u.l per-unit-length. 17, 19, 28, 29

pdf probability density function. 34, 35

PLC power line communication. i, ii, ix, xi, 1, 2, 6–11, 13, 22, 33, 39, 40, 45, 49, 61, 62

PSD power spectral density. ix, 32–36

QPSK quadrature phase shift keying. 45

RF radio frequency. 26

RMS root mean square. 15, 62

SDO standards developing organisation. 8, 9

SINR signal-to-interference-noise ratio. ix, x, 10, 11, 39, 41, 42, 44–47, 49, 50, 54–59, 62

SIR signal-to-interference ratio. ix, 31, 32, 37, 42, 44, 46

SNR signal-to-noise ratio. 42, 44–46, 55, 59

SOE sum-of-exponentials. vi, vii, 53, 54, 58, 60

SONR *useful signal* to out-of-band interference noise ratio. vi, vii, 50, 52–56, 58, 59, 62, 65, 66

UNB ultra narrowband. 8, 9

WAN wide area network. 6

WLAN wireless local area network. 6

WSSUS wide-sense stationary uncorrelated scattering. 63

ZF zero forcing. i, 10, 43–47, 54

Chapter 1

Introduction

1.1 Motivation

To combat the ongoing severe environmental problems and achieve higher reliability and safety of the electricity power grid, many government agencies around the world are deploying ubiquitous projects on developing the next-generation power grid: the smart grid. By utilizing modern information and communication technologies, smart grid is capable of delivering power in more efficient and green ways, and responding to a variety of normal or emergency conditions and events [7]. Smart metering is an enabling technology in the smart grid to address the energy wasting problem. It monitors and optimizes the power consumption of consumers' devices and appliances. To ensure proper operation of smart metering, a reliable communication infrastructure plays a crucial role. Different kinds of communication technologies, such as wireless communication, power line communication (PLC) and optical communication, will be used cooperatively to build up this communication infrastructure.

Recently, PLC has attracted a lot of attention since it is the only wired communication technology which has a deployment cost comparable to wireless communication. It can also be maintained by the power company itself other than a third party service provider. PLC in a smart grid is responsible for the communication between smart meters and home appliances, as well as the communication between smart meters and power companies. The latter link is an access network which is only for data transmission while the former link is more like a sensor network which has monitoring and controlling capabilities. Such a network will also enable the future smart home applications, including Internet-of-things. However, communication in such a network using PLC is challenging due to a variety of channel impairments [8]. Motivated by this, this MPhil research aims at developing low-cost PLC solutions which are robust to those channel impairments for the emerging smart grid applications.

To understand those impairments, extensive study on the characterisation and modelling of power line channel has been conducted. It was found that indoor power line channel between the smart meter and appliances may be time-varying [9], and such a

behaviour may cause significant intercarrier interference (ICI) [10] to a multi-carrier system like orthogonal frequency division modulation (OFDM). However, ICI mitigation capability is absent in existing PLC standards for smart grid applications. Hence, these standards may suffer from severe performance degradation if no proper action is taken at the receiver. It was found that the banded equaliser with time-domain receiver windowing may be a good low-cost solution. These techniques have been well studied in wireless communication. However, our research revealed that some receiver window design criteria developed for wireless communication do not work properly over power line channels. Therefore, in this thesis we propose an alternative solution to receiver window design for PLC.

1.2 Contributions

Our research has produced two main contributions:

- Extensive investigation on power line channel characterisation and modelling has been conducted and a review paper has been published [11]. To assist the development and verification of the proposed window design criterion, a two-conductor transmission line (2TL) based indoor time-varying power line channel simulation tool was developed by adopting the voltage ratio approach proposed in [12] and the time-varying channel model proposed in [5]. This tool was implemented with MATLAB®. The key feature of this tool is that it accepts any tree-structured power network topology and a variety of load models. In addition, it can be extended to generating multi-conductor transmission line (MTL) based power line channels.
- Banded OFDM with time-domain receiver windowing was investigated over time-varying power line channel for the purpose of ICI mitigation. It is the first time such a study has been done for PLC. The key finding is that some good window design criteria [13, 14] proposed for wireless communication do not work well over power line channels due to the time variation of power line channel energy. To fill this gap, we propose an alternative window design criterion. Simulations have shown that the proposed criterion outperforms the other criteria in terms of bit error rate (BER) reduction. It also presents a few advantages.

1.3 Thesis Overview

In chapter 2 we provide some background information about smart grid and PLC. We focus on the significance and design challenges of PLC for smart grid applications. We also review some existing works on OFDM systems design over time-varying power line channels and wireless channels, respectively.

In chapter 3 we first present a review of power line channel modelling approaches, including the top-down approach and the bottom-up approach. After that we introduce the 2TL theory and the MTL theory. These two theories are the fundamentals of bottom-up approaches. Based on the 2TL theory, we present a time-varying power line channel model as well as some key issues regarding its implementation as a simulation tool. Finally, we review some representative noise models.

In chapter 4 we investigate the performance of some well-known linear equalisers over time-varying power line channels. The main purpose is to show the significance of ICI. We first describe the system model of an OFDM system over time-varying channel. Then we present some simple analyses on ICI followed by a description of those linear equalisers. Finally, the error performances of those equalisers are investigated via simulation.

Chapter 5 presents our investigation on receiver window design over time-varying power line channel. We first demonstrate the algorithms of the two well-known window design criteria proposed for wireless communication and then we propose an alternative window design criterion. With the assistance of simulation, we analyse these criteria and point out the advantages of our proposal. We also analyse the effect of some key parameters used in window design.

Chapter 6 concludes this thesis and points out some possible future research directions.

1.4 Publications

1. W. Zhu, X. Zhu, E. G. Lim, and Y. Huang, "State-of-art power line communications channel modelling," *Procedia Computer Science*, vol. 17, no. 0, pp. 563 - 570, 2013.

2. W. Zhu, X. Zhu, E. G. Lim, and Y. Huang, "Receiver Window Design for OFDM Systems over Time-Varying Power Line Channels," *the 10th International Conference on Wireless Communication, Networking and Mobile Computing*, Beijing, Sep. 2014.

1.5 Notations

The following notations are used in this thesis.

$[\mathbf{B}]_{m,n}$	the element in the m^{th} row and n^{th} column of matrix $\mathbf{B}$
$[\mathbf{B}]_m$	the m^{th} row of matrix $\mathbf{B}$
$(\cdot)^T$	matrix or vector transpose
$(\cdot)^H$	Hermitian transpose
$(\cdot)^*$	complex conjugate
$\mathbf{I}_N$	an $N \times N$ identity matrix
$\mathbf{0}_{M\times N}$	an $M \times N$ matrix with all zero elements
$\langle\cdot\rangle_N$	modulo-N operation
$\mathrm{E}[\cdot]$	expectation
$\|\cdot\|_F$	Frobenius norm
$\mathcal{D}(\mathbf{B})$	a diagonal matrix that has the same diagonal as $\mathbf{B}$
$\mathcal{D}(\mathbf{b})$	a diagonal matrix with diagonal $\mathbf{b}$
$\circ$	element-wise multiplication
$\lceil\cdot\rceil$	ceiling
$\mathrm{tr}\{\cdot\}$	trace

Chapter 2

Research Overview

2.1 Smart Grid and Smart Metering

Smart grid is envisioned as the next-generation power grid with improved efficiency, reliability and safety. Traditional power grids transmit power from a few central generators to a large number of consumers while smart grid applies two-way flows of electricity and information to create an automated and distributed energy delivery network. Smart grid is achieved by incorporating advanced information and communication technologies with distributed green energy generations and intelligent management systems. Many applications will be enabled by smart grid, such as [7]:

- Fault detection, diagnosis and recovery: the faults in a power grid caused by man-made mistakes or natural disasters can be detected and diagnosed by the grid itself without any human assistance. Depending on the situation, different strategies will be performed in order to minimize the probability of black-outs.
- Marketisation of electricity: thanks to the two-way transmission of electricity, consumers will be able to sell electricity to power companies hence influencing the price of electricity.
- Automatic meter reading: the power consumption information will be sent to power companies by smart meters automatically.
- Demand response: smart meters control the operation of appliances according to users' demand and electricity price so as to minimize the total cost on electricity.

The above applications are supported by the so-called automatic metering infrastructure (AMI), which is widely regarded as a logical strategy to realize smart grid. Smart meters, which support two-way communication between meters and power companies, are regarded as part of the AMI. A smart meter is usually an electrical meter that records power consumption in intervals of an hour or less and sends that information at least daily back to the utility for monitoring and billing purposes [7]. Home energy management system (HEMS) is the most important application of a smart meter. It monitors and optimises all kinds of energy consumption and production within a home.

This usually involves the operation of electric cars, home appliances, green energy generations such as solar panels and other forms of energy and resources including gas and water.

2.1.1 Communication Infrastructures for Smart Grid

An efficient and reliable communication infrastructure is one of the keys to realise the envisioned smart grid applications. Due to the real-time nature of the operation of smart grid, the communication infrastructure should be able to correctly deliver a large number of messages in time. This brings up some key requirements of communication over smart grid. They are low latency, high reliability and high throughput. In addition, due to massive deployment of smart meters, the design of smart meters should also focus on low complexity and low cost.

Logically, smart grid is a huge network with different layers. The bottom layer is for power delivery while other layers are for communication and management. It is generally agreed that the communication network of a smart grid should contain home area networks (HANs) that connect home appliances to smart meters, neighbourhood area networks (NANs) that collect messages from all the smart meters within them and wide area networks (WANs) that forward messages from NANs to power companies or vice versa [15–17]. The whole network is an integration of different communication technologies in terms of the operating environment. For example, 3G, 4G technologies or optical fibres can be used for WANs and NANs while wireless local area network (WLAN) and PLC technologies can be adopted for HANs and NANs.

PLC and ZigBee[1] have been widely investigated and generally agreed as two promising candidates for smart grid applications in HANs and NANs. The main advantage of PLC is that the communication medium (the power line) is already there hence it is the only wired technology that has a deployment cost comparable to wireless communication (e.g. Zigbee). Various studies have shown that PLC can provide a very good performance, especially when OFDM is applied [18–20]. ZigBee is also a very good candidate due to its low power consumption and flexible configuration. However, ZigBee is a very mature technology while the development of PLC is more attractive. Therefore, PLC has been chosen as the technology that is studied in this research.

2.2 Power Line Communication

2.2.1 Network Structure

The structure of a power grid is illustrated in Fig. 2.1. A power grid usually contains high-voltage (HV) transmission networks, medium-voltage (MV) distribution networks and low-voltage (LV) distribution networks. HV networks deliver power from power

[1]ZigBee Alliance, available online at: http://www.zigbee.org/.

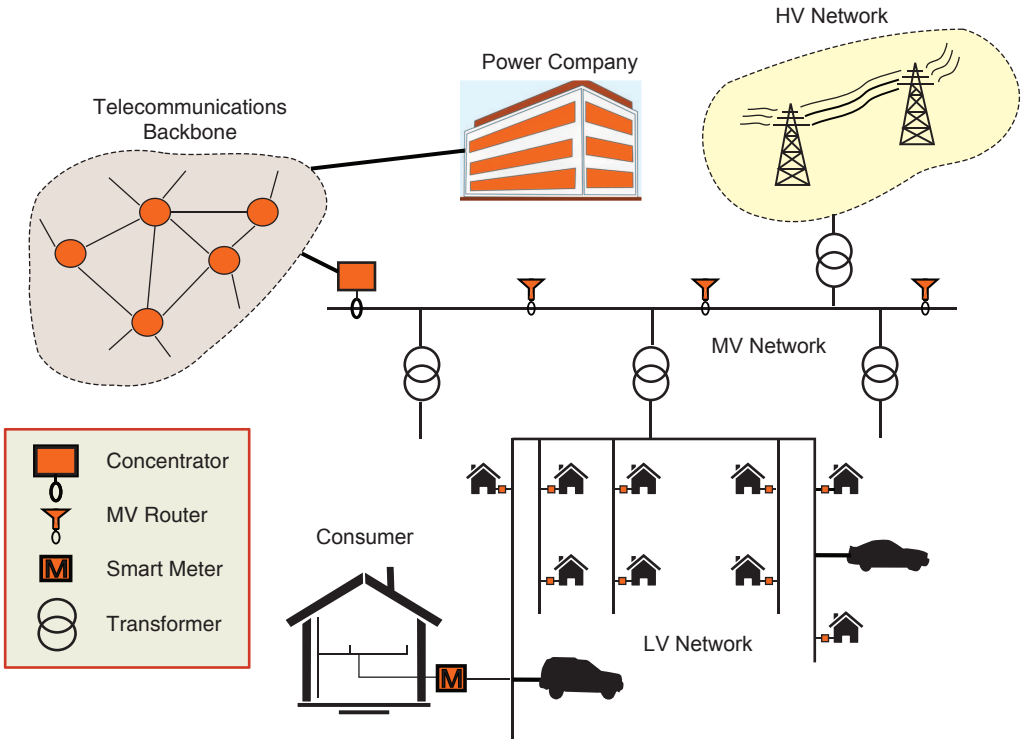

Fig. 2.1: A PLC based communication infrastructure for smart grid [1]

plants to populated areas. MV networks distribute power in a large scale and LV networks distribute power to end-users.

Most of the time, PLC is used in LV and MV networks. Comparing with the logical structure of smart grid, a HAN refers to the communication within a home (LV as well) and it is coordinated by a smart meter. A NAN refers to the communication within a LV network or across both LV and MV networks. Routers are deployed if necessary. A concentrator is usually located in a MV network. It collects all the data within that area and forwards it to the power company through a telecommunication backbone network. The backbone network may be a 3G, 4G or fibre optics network.

In this thesis, we consider the communication within a HAN. A typical layout of HAN is shown in Fig. 2.2. A smart meter is usually located at the service panel where the indoor power network is connected to the outdoor LV network. The indoor power network spreads out from the service panel like a tree and appliances, lights and outlets are connected to the network. In the future, home appliances will be intelligent and able to communicate with the smart meter. Different appliances or lights response to the power supply differently. This is the main cause of channel time variation.

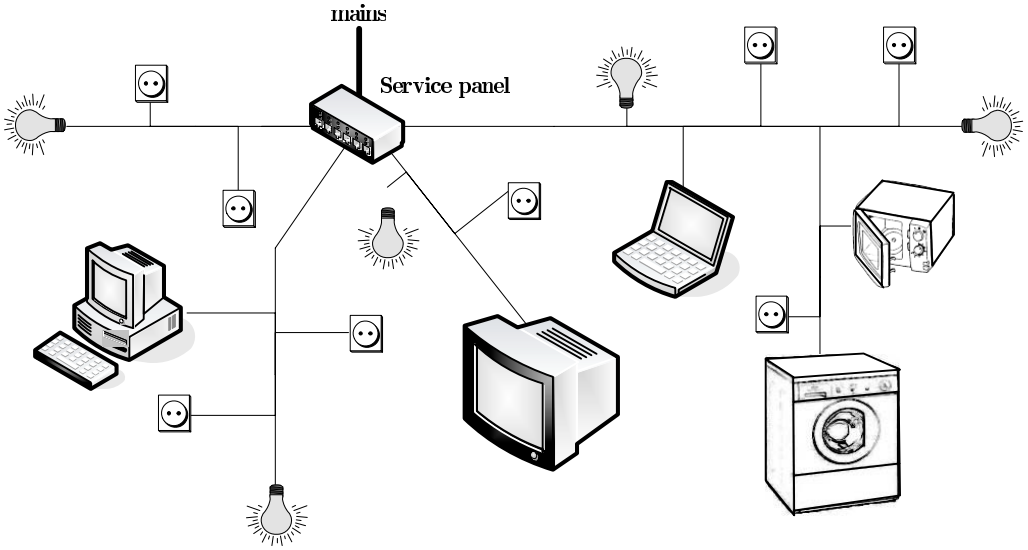

Fig. 2.2: A typical home area network [2]

2.2.2 History and Developments

PLC technologies can be divided into three classes in terms of their operational bandwidth: ultra narrowband (UNB), narrowband (NB) and broadband (BB) [8]. These three classes and their data rates, bandwidths are summarised in Table 2.1. Generally, UNB-PLC provides a very low data rate but a very large communication range (150 km or more) because it has a small path loss coefficient and it is easy to pass through transformers. UNB-PLC solutions are very mature technologies that have been in the field for at least two decades. NB-PLC solutions provide higher data rates but a smaller communication range than UNB-PLC. NB-PLC can be further divided into low data rate (LDR) NB-PLC and high data rate (HDR) NB-PLC depending on whether single carrier or multiple carriers are used. There is a variety of LDR NB-PLC recommendations available today. The development of HDR NB-PLC solutions has been in progress for several years. Two commercial initiatives are PRIME[2] and G3-PLC[3]. Two standards developing organisation (SDO)-based standards are ITU-T G.hnem (G.9955/G.9956) and IEEE 1901.2. BB-PLC has the highest data rate but a very small communication range (normally limited to HANs) because of its high frequency components. IEEE 1901 and ITU-T G.hn (G.9960/G.9961) are two famous SDO-based recommendations.

According to [8], NB-PLC is the best choice for smart grid applications than other PLC technologies for the following reasons:

[2]Powerline Related Intelligent Metering Evolution, available online at: http://www.prime-alliance.org/.

[3]Open Standard for SmartGrid Implementation, available online at: http://www.maxim-ic.com/products/powerline/g3-plc/.

Table 2.1: Technical specifications of three PLC classes

PLC Class	Data Rate	Bandwidth
UNB	around 100 bps	0.3-3 kHz or 30-300 Hz
NB	LDR: a few kbps; HDR: up to 500 kbps	3-500 kHz
BB	several hundred Mbps	1.8-250 MHz

- The CENELEC band (3-148.5 kHz) used by NB-PLC is the only PLC band that is available all over the world.
- NB-PLC has a moderate coverage and it can pass through transformers.
- HDR NB-PLC standards are designed explicitly for smart grid applications.
- NB-PLC can coexist with BB-PLC via frequency-division multiplexing so that they can be deployed in the same network while providing different services.

Due to the above reasons and in order to be consistent with the SDO-based PLC standards, HDR NB-PLC and the frequency band 3-500 kHz is considered in this thesis. OFDM is commonly adopted in existing HDR NB-PLC standards. Therefore, it should be expected that these standards may suffer from ICI when they are used over time-varying power line channels.

2.2.3 Research Challenges

We have identified four major challenges regarding the research of PLC over HANs. First of all, power line channel modelling is very challenging. As will be discussed in chapter 3, there is no universally recognised power line channel model. Since a reliable channel model is of paramount importance to good studies of communication technologies, this shortage significantly impedes the development of a good PLC technology. Existing PLC technologies are mostly migrated from wireless communication with little mathematical justification. Second, the complex impulsive noise scenario is a special and unique challenge to PLC system design. As will be introduced in chapter 3, there is a variety of impulsive noise in power line channels, especially in HANs due to the presence of appliances. When it occurs, a number of data symbols or even a whole packet may be corrupted. Third, indoor power line channels may present a time-varying behaviour. Power line channel time variation is composed of long term variations caused by random topology change, such as plug-in and plug-out of appliances, and short term variations due to load variations [9]. Long term variations require adaptive algorithms which can sense the sudden change of channel. Short term variations may cause significant ICI to multi-carrier systems such as OFDM. Finally, power line signals may interfere with some low frequency radio signals due to the antenna-like behaviour of transmission lines. This problem leads to performance degradation to both PLC and radio communication.

2.3 OFDM Systems over Time-Varying Channels

The time-varying behaviour of power line channel appears to be an interesting research subject. Since OFDM is widely used in NB-PLC standards, we choose to investigate the ICI mitigation ability of OFDM systems over time-varying indoor power line channels.

2.3.1 OFDM Communications Overview

OFDM is a kind of multicarrier modulation technique which relies on parallel data transmission in the frequency domain. It is extremely simple and efficient over linear time-invariant (LTI) frequency-selective channels. In OFDM systems, data symbols are transmitted on equispaced frequencies called subcarriers. When properly designed, each subcarrier occupies a narrow bandwidth so that its corresponding subchannel can be seen as frequency-flat. When cyclic prefix (CP) is incorporated, the subcarriers are orthogonal to each other such that not only inter-symbol interference (ISI) is absent, but also there is no ICI among subcarriers. As a result, equalisation is very simple in OFDM systems over LTI channels.

However, when the channel experiences a non-negligible time variation, each subcarrier suffers a Doppler spreading effect which destroys the orthogonality between subcarriers, hence producing significant ICI. Similar to ISI in single-carrier systems, the presence of ICI decreases signal-to-interference-noise ratio (SINR) and, when left uncompensated, it degrades the performance of OFDM systems. A simple solution is to shorten the OFDM block length so that less channel variation, hence reduced ICI power, is experienced. However, since CP has to be inserted for each OFDM block, this method reduces information throughput. Therefore, other ICI mitigation techniques are necessary.

2.3.2 ICI Mitigation Techniques

A few but not many studies regarding the characterisation of power line channel time variation can be found in literature. Some good work can be found in [9, 10]. Measurement results in [9] reveal that Doppler spread of indoor power line channels can be as large as 1700 Hz. With such a high Doppler spread, ICI may cause serious performance degradation to OFDM based NB-PLC systems. The work in [10] derived a formula for the SINR of an OFDM block. Based on this result, an algorithm that optimises OFDM block size was developed. Unfortunately, studies on error performance and ICI mitigation of an OFDM system over time-varying power line channel can hardly be found.

ICI mitigation of OFDM has been well investigated in wireless communication. Solutions include linear equalisers like zero forcing (ZF), minimum mean squared error (MMSE) and banded equalisers, and non-linear equalisers such as decision feedback

equalisers, maximum likelihood (ML) equalisers and turbo equalisers [21]. Among them, banded equalisers provide a better tradeoff between performance and complexity. Banded equalisers are usually assisted by receiver windows which enhance the accuracy of banding. Two well-known receiver window design criteria can be found in [13, 14]. The one proposed in [13] attempts to maximise the modified input SINR while the other one tries to minimise the band approximation error (BAE). These two criteria work very well over time-varying wireless channels. However, when they are applied for time-varying power line channels, their performance degrade dramatically. To the best of our knowledge, there is no publication regarding receiver window design for the purpose of ICI mitigation over time-varying power line channels. Therefore, we believe such a study is necessary for PLC.

Chapter 3

Power Line Channel and Noise Models

Power line channel is a very harsh electronic communication media which poses a number of challenges to communication system design. First, it is frequency selective due to signal reflections and transmissions caused by impedance mismatches at transmission line discontinuities. Although physical behaviours of reflections and transmissions are well studied in transmission line theory, statistical behaviours are not well characterised. Second, it exhibits high attenuation and strong low-pass behaviours which limit not only network coverage but also usable frequency bands. These two problems exist because transmission lines are not designed for transmissions of high frequency signals. Normally, due to complex network topologies and thin cables, indoor power line channels present higher attenuation than outdoor channels. Third, it may be time-varying because of different kinds of network variations including change of topology, variation of loads and fluctuation of cable parameters. This is usually true for indoor power line channels due to the time-varying behaviour of electronic appliances. Apart from these, PLC systems are further impaired by coloured background noise and complex impulsive noise. Therefore, extensive studies on channel characterisation and modelling are necessary for efficient utilisation of the channel.

Unfortunately, it is not easy to conduct research on power line channel or develop universally recognised channel models. The reasons are twofold. On the one hand, the structure of power grid varies from place to place. For example, two-phase configuration is common in the United States but not in Europe while three-phase configuration is common in Europe [2]. This impedes the development and standardisation of a generally applicable channel model, especially a statistical one. On the other hand, channel measurement is dangerous because of the high voltage. Critical isolation of the mains voltage is required for protection and signal extraction. Apart from safety reasons, outdoor channel measurement requires authorisation and assistance from power companies.

Nevertheless, great efforts have been made to power line channel modelling. Two

kinds of modelling approaches can be found in the literature, namely the top-down approach [22–26] and the bottom-up approach [5, 12, 27–37]. A top-down approach attempts to find the most fitted model from measurements (either impulse responses or frequency responses), while in a bottom-up approach the channel model is derived from transmission line theory. The channel model used in this thesis is a kind of bottom-up model which models the periodic time-varying behaviour of indoor power line channels.

In this chapter, we first review the top-down and bottom-up channel modelling approaches. Then we introduce the 2TL theory and the MTL theory [4], as well as the transfer function computation methods proposed in [12] and [33]. After that, we explain in details the time-varying channel model [5] that is adopted in this thesis. Based on this model, a simulation tool is implemented. Some key issues regarding implementation, along with some representative simulation results, are demonstrated afterwards. Finally, we review some representative coloured background noise models and impulsive noise models.

3.1 Review of Channel Modelling Approaches

3.1.1 Top-Down Approaches

Top-down approaches aim at developing statistical channel models through data fitting. This kind of approach originates from wireless communication but as mentioned before, data collection and characterisation of power line channels are more difficult than that of wireless channels. Therefore, although great efforts have been made on channel measurement, a complete practical channel model is yet to be found.

The advantage of a statistical model is its low complexity. Once the model and parameters are given, numbers of channel realisations can be generated within a short period of time. In addition, with the help of statistical results derived from measurements, channel and even system performance may be studied analytically. The most significant disadvantage is its low flexibility. The model and parameters derived for a specific network or a frequency band may not be applied to other networks and frequency bands. Another disadvantage is that it lacks physical connection with reality. For example, it is hard to describe the possible spatial correlation presented between neighbouring nodes in a power network with a statistical model.

The most famous top-down model is proposed in [23] by Zimmermann and Dostert. It models the channel in frequency domain as a sum of multiple signal paths with different amplitudes, phases and delays. The transfer function of a channel can be expressed as

$$H(f) = \sum_{i=1}^{N} g_i e^{-(a_0 + a_1 f^k) d_i} e^{-j2\pi f (d_i / v_p)} \tag{3.1}$$

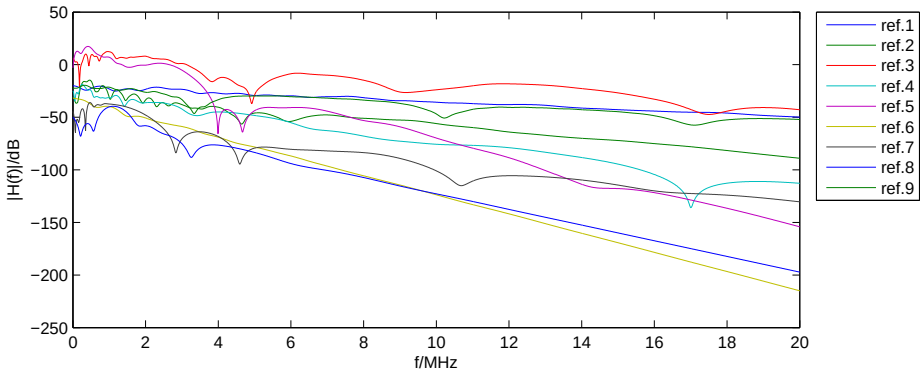

Fig. 3.1: Frequency responses of the OPERA reference channels [3]

where N is the number of dominant paths, g_i is the weight of the i^{th} path which accounts for the total effect of reflections and transmissions, a_0 and a_1 represents the attenuation of cable, k determines the dependency of attenuation on frequency f, d_i is the length of the i^{th} path, and v_p is the phase velocity of the cable.

In order to use this model, a set of parameters should be given. Based on the authors' measurements, they defined several reference channels with respect to link distances. Additionally, the Open PLC European Research Alliance (OPERA) project [3] proposed 9 reference channels for LV and MV networks based on this model. Fig. 3.1 shows the channel transfer functions of these reference channels. The low-pass behaviour is clearly seen from this figure.

A major drawback of this model is that the computational cost for determining the dominant paths and the corresponding parameters grows fast with the number of dominant paths. In indoor environments, there are usually a large number of paths and the attenuation is low due to short path length. As a result, many strong paths may present, causing a high computational cost. In this sense, a statistical model seems more convenient. This was first achieved by Tonello's team in [25] where the model is extended statistically and 9 sets of parameters corresponding to the 9 reference channels in [3] are provided.

Many other top-down channel model proposals can be found in literature. Based on extensive measurements, Tlich et. al. [26] proposed a random channel model in frequency domain by analysing statistical properties of the magnitude and phase of the measured channel transfer functions. On the contrary, the channel model proposed by Galli [22] is based on time domain statistics, such as average channel gain and root mean square (RMS) delay spread.

3.1.2 Bottom-Up Approaches

The bottom-up approach is usually based on transmission line theory [4]. This approach requires perfect knowledge of the targeting power network, including its topology, power

cables and loads. These network elements are modelled mathematically so that they can be incorporated to generate channel realisations. A bottom-up approach usually contains two steps of work. First, signal propagation in a single piece of transmission line is understood based on transmission line theory. Depending on the technique used, signal propagation can be described by voltage, current or s-parameters. Second, after dividing the network into many pieces of transmission lines, the channel realisation can be obtained by cascading the effect of these pieces.

The advantage of a bottom-up approach is that it can be applied to various situations as long as the network information is available. In addition, this approach is closely related to the physics of signal propagation in power networks. Therefore, it can be applied to network-related system modelling such as multiuser systems and relay systems. This approach also has several disadvantages. First, it is usually computational complex and the complexity grows with the complexity of the network. Second, the collection of the aforementioned network elements is challenging and time consuming.

Most of the bottom-up approaches in the literature are based on one of the three techniques, namely the voltage ratio approach [12, 27–30, 33], the ABCD matrix approach [5, 31, 37] and the s-parameters approach [34–36]. The voltage ratio approach and the ABCD matrix approach are essentially the same because the voltage ratio approach describes the relationship between input voltage and output voltage while ABCD matrix describes the input/output relationship of both voltage and current. The voltage ratio approach developed for 2TL in [12] is extensively used in our simulation and will be introduced later in this chapter. We refer readers to [37] for a good work on ABCD matrix based channel modelling approach. The s-parameters approach is different. It describes electromagnetic (EM) wave propagation with transmission and reflection coefficients other than voltage and current. Although this approach is complicated, it can be easily extended to the situation where different kinds of cables with different number of conductors are connected together. On the contrary, it is hard for a voltage ratio approach or an ABCD matrix approach to be applied to this situation. We refer readers to [34] for a good demonstration of this approach. An exception of bottom-up approach can be found in [32] where the model is basically a multipath model partly cooperated with the transmission line theory.

3.1.3 The Future of Power Line Channel Modelling

Power line channel modelling and characterisation is still an open and challenging research topic. There are a few rules that can be regarded as guidances of the future development of such a subject.

First of all, a fast and flexible random channel generation tool essentially helps the development of PLC. Traditionally, a time domain top-down channel model based random channel generation tool usually requires statistical information such as amplitude

distribution, power delay profile, RMS delay spread, etc.. However, these information is not available for PLC nowadays. Some similar frequency domain statistical information can be found in [25] while it is yet to be improved and extended in order to make the model generally applicable. In addition to these statistical information, it would be much better if the model considers channel time variation and spatial correlation. Two kinds of spatial correlation can be found in a power network, namely the spatial correlation between power line conductors and the spatial correlation between users. A study on spatial correlation between conductors can be found in [38] while no research on spatial correlation between users was found. Nevertheless, it is not hard to image that such kinds of work could be very challenging. More importantly, statistical information helps evaluating theoretical performance of a communication system. Hence, it is importance to acquire these information and generalise them for a variety of application scenarios.

Secondly, the development of multiple-input-multiple-output (MIMO) power line channel model may change the future of PLC since in most cases outdoor power networks use MTLs. As mentioned above, there are already a variety of bottom-up channel models that supports MIMO power line channel modelling. However, a MIMO top-down channel model is yet to be found. The characterisation of coupling between conductors can be very challenging for a top-down approach. In addition, the impedance of a load that is connected to a MTL network also needs to be characterised because such a kind of information is usually not available.

Finally, the most significant problem of channel modelling for smart grid communications is the lack of narrowband channel models. Most of the channel models, especially top-down ones, are broadband channel models in the frequency band of 1-100 MHz. Very few of them focus on or cover the European Committee for Electrotechnical Standardization (CENELEC) bands (3-500 kHz). The study of outdoor power line channel modelling is of paramount importance for smart grid because outdoor power networks will support the communication between smart meters and central offices with very high reliability. Spatial correlation between users can also be a very interesting research direction since a large number of smart meters and sensors will share the same network. If correlation information between meters and sensors can be utilised, communication system design may be simplified. In addition, this may also help the design of relay systems.

3.2 Transmission Line Theories

Transmission line theories are the fundamentals of bottom-up approaches. They explain signal propagation in transmission lines from the very basic EM point of view. Depending on the number of conductors in a transmission line, there are 2TL theory and MTL theory. In this section we explain how to use these theories to calculate the

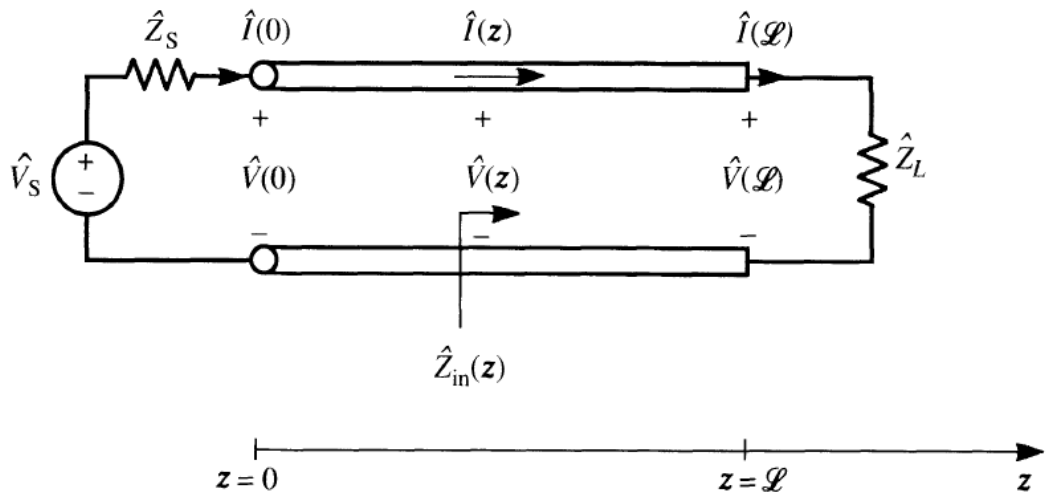

Fig. 3.2: A two-conductor transmission line model [4]

transfer function of a transmission line. Then we show how to use the voltage ratio approach proposed in [12] and [33] to compute the overall transfer function between two terminals of a power network.

3.2.1 The Two-Conductor Transmission Line Theory

This subsection considers transfer function calculation of a 2TL. 2TL theory considers any transmission line that has two conducting wires, such as twisted-pair cables and coaxial cables, as shown in Fig. 3.2. In this figure, the two wires are excited by a voltage source V_S with impedance Z_S and terminated by a load Z_L. The line has a length of $\mathscr{L}$.

This kind of circuit cannot be solved by the conventional Ohm's law because the voltage and current along the line are not constants. In order to obtain the voltage and current distribution, the line is uniformly divided into an infinite number of segments and the voltage and current are assumed to be constant within each segment. This assumption is only valid when the length of each segment is infinitesimal. An equivalent circuit then can be formed for each segment of cable, as shown in Fig. 3.3. In this figure, Δz denotes the length of each segment and r, l, g and c are called the per-unit-length (p.u.l) resistance, inductance, conductance and capacitance of the line respectively.

Applying Kirchhoff's voltage and current laws to the circuit, the following voltage and current relationships can be found

$$V(z+\Delta z,t) - V(z,t) = -r\Delta z I(z,t) - l\Delta z \frac{\partial I(z,t)}{\partial t} \tag{3.2}$$

$$I(z+\Delta z,t) - I(z,t) = -g\Delta z V(z+\Delta z,t) - c\Delta z \frac{\partial V(z+\Delta,t)}{\partial t} \tag{3.3}$$

Dividing both sides by Δz and taking the limit as $\Delta z \to 0$ yields the time domain

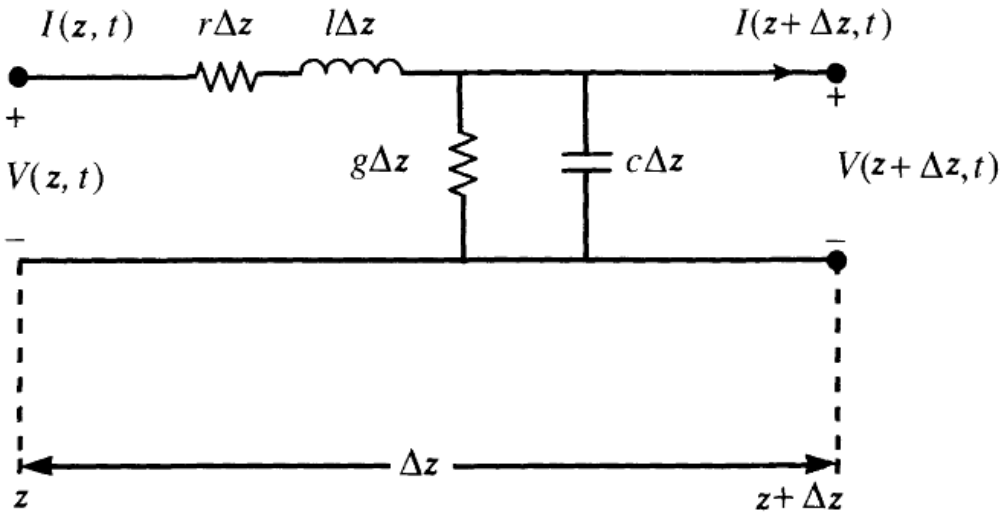

Fig. 3.3: The per-unit-length equivalent circuit for a two-conductor line [4]

transmission line equations

$$\frac{\partial V(z,t)}{\partial z} = -rI(z,t) - l\frac{\partial I(z,t)}{\partial t} \tag{3.4}$$

$$\frac{\partial I(z,t)}{\partial z} = -gV(z,t) - c\frac{\partial V(z,t)}{\partial t} \tag{3.5}$$

The frequency domain equivalents of these two equations can be expressed by

$$\frac{\mathrm{d}}{\mathrm{d}z}V(z) = -ZI(z) \tag{3.6}$$

$$\frac{\mathrm{d}}{\mathrm{d}z}I(z) = -YV(z) \tag{3.7}$$

where $V(z)$ and $I(z)$ denote the voltage and current at position z along the line, $Z = r + j\omega l$ and $Y = g + j\omega c$ are the p.u.l impedance and admittance of the line respectively, and $\omega = 2\pi f$ is the radian frequency.

The solutions (see chapter 5 of [4]) are expressed as

$$V(z) = V^+ e^{-\gamma z} + V^- e^{\gamma z} \tag{3.8}$$

$$I(z) = \frac{V^+}{Z_C} e^{-\gamma z} - \frac{V^-}{Z_C} e^{\gamma z} \tag{3.9}$$

where V^+ and V^- represents the voltages of the forward-travelling wave and backward-travelling wave, $Z_C = \sqrt{Z/Y}$ is the characteristic impedance of the line, $\gamma = \sqrt{ZY} = \alpha + j\beta$ is the propagation constant with α and β as the attenuation constant and phase constant respectively. The phase velocity then can be calculated by $\nu = \omega/\beta$.

The backward-travelling waves are caused by signal reflection at the load. To quantify this reflection, the reflection coefficient is defined as the ratio of backward-travelling

wave to forward-travelling wave, as expressed by

$$\Gamma(z) = \frac{V^- e^{\gamma z}}{V^+ e^{-\gamma z}} = \frac{V^-}{V^+} e^{2\gamma z} \tag{3.10}$$

Then (3.8) and (3.9) can be rewritten as

$$V(z) = V^+ e^{-\gamma z}(1 + \Gamma(z)) \tag{3.11}$$

$$I(z) = \frac{V^+}{Z_C} e^{-\gamma z}(1 - \Gamma(z)) \tag{3.12}$$

Incorporating the load impedance using $V(z)/I(z) = Z_L$, the reflection coefficient at load can be obtained as

$$\Gamma_L = \Gamma(\mathscr{L}) = \frac{Z_L - Z_C}{Z_L + Z_C} \tag{3.13}$$

The input impedance at any position along the line can be obtained in a similar way and it is expressed by

$$Z_{in}(z) = \frac{V(z)}{I(z)} = Z_C \frac{1 + \Gamma(z)}{1 - \Gamma(z)} \tag{3.14}$$

The input impedance at the input of the line ($z = 0$) is

$$Z_{in}(0) = Z_C \frac{1 + \Gamma_L e^{-2\gamma\mathscr{L}}}{1 - \Gamma_L e^{-2\gamma\mathscr{L}}} = Z_C \frac{Z_L + Z_C \tanh(\gamma\mathscr{L})}{Z_C + Z_L \tanh(\gamma\mathscr{L})} \tag{3.15}$$

Finally, by incorporating $V_S = I(0)Z_S + V(0)$, we can obtain the voltage and current distribution on the line, as expressed by

$$V(z) = \frac{1 + \Gamma_L e^{-2\gamma\mathscr{L}} e^{2\gamma z}}{1 - \Gamma_S \Gamma_L e^{-2\gamma\mathscr{L}}} \frac{Z_C}{Z_C + Z_S} V_S e^{-\gamma z} \tag{3.16}$$

$$I(z) = \frac{1 - \Gamma_L e^{-2\gamma\mathscr{L}} e^{2\gamma z}}{1 - \Gamma_S \Gamma_L e^{-2\gamma\mathscr{L}}} \frac{1}{Z_C + Z_S} V_S e^{-\gamma z} \tag{3.17}$$

where $\Gamma_S = (Z_S - Z_C)/(Z_S + Z_C)$ is the reflection coefficient at source. The transfer function, defined as the ratio of $V(\mathscr{L})$ to $V(0)$, is then given by

$$H_0(f) = \frac{V(\mathscr{L})}{V(0)} = \frac{1 + \Gamma_L}{e^{\gamma\mathscr{L}} + \Gamma_L e^{-\gamma\mathscr{L}}} \tag{3.18}$$

If we consider the source voltage, the transfer function is given by

$$H(f) = \frac{V(\mathscr{L})}{V_S} = \frac{1 + \Gamma_L}{1 - \Gamma_S \Gamma_L e^{-2\gamma\mathscr{L}}} \frac{Z_C}{Z_C + Z_S} e^{-\gamma\mathscr{L}} \tag{3.19}$$

In fact, (3.19) is reduced to (3.18) when $Z_S = 0$. In [12], (3.18) is used to calculate the channel transfer function, but we believe (3.19) is a better choice since it considers the effect of source reflection. It is important to note that (3.13), (3.15), (3.18) and (3.19) are four key equations that are used in channel transfer function calculation. In addition, the channel transfer function is frequency dependent because almost all the p.u.l parameters are frequency dependent and some loads can be frequency dependent as well. For convenience, frequency dependency is omitted in the equations.

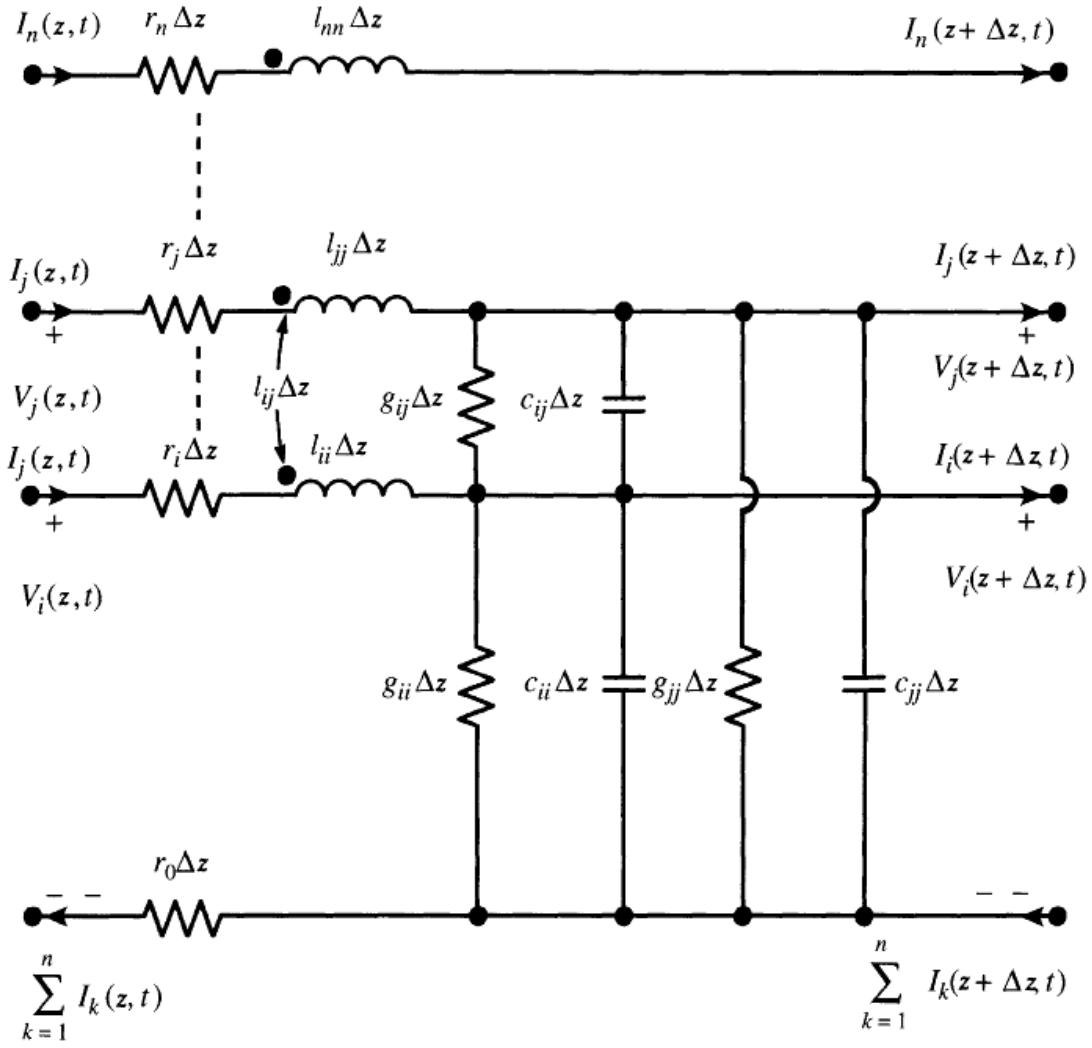

Fig. 3.4: The per-unit-length equivalent circuit of a multi-conductor transmission line [4]

3.2.2 The Multi-Conductor Transmission Line Theory

MTL theory was developed for transmission lines with more than two conductors. This kind of transmission line is commonly used in outdoor power networks to distribute power in three phase. Therefore, four conductor (one neutral line plus three phase lines) and five conductor (with an additional ground line) transmission lines are common commercial products. Sometimes three conductor transmission lines are used in indoor environments and the additional conductor is for grounding.

The voltage and current in a MTL are defined in vector forms as $\mathbf{v}(z)$ and $\mathbf{i}(z)$. Suppose there are n conductors, then $\mathbf{v}(z)$ and $\mathbf{i}(z)$ are all $n \times 1$ column vectors where $\mathbf{v}(z)$ contains the voltages between every two conductors and $\mathbf{i}(z)$ contains the current

flow in each conductor. Voltages and currents are related by

$$\frac{\mathrm{d}}{\mathrm{d}z}\mathbf{v}(z) = -\mathbf{Z}\mathbf{i}(z) \tag{3.20}$$

$$\frac{\mathrm{d}}{\mathrm{d}z}\mathbf{i}(z) = -\mathbf{Y}\mathbf{v}(z) \tag{3.21}$$

where $\mathbf{Z} = \mathbf{R}+j\omega\mathbf{L}$ and $\mathbf{Y} = \mathbf{G}+j\omega\mathbf{C}$ are the p.u.l impedance matrix and admittance matrix, respectively, $[\mathbf{L}]_{i,j}$, $[\mathbf{G}]_{i,j}$, $[\mathbf{C}]_{i,j}$ are defined in Fig. 3.4, and $\mathbf{R} = \mathcal{D}([r_1, \ldots, r_n]) + r_0$ with $[r_0, \ldots, r_n]$ defined in Fig. 3.4. These two equations can not be solved directly because voltages and currents are coupled.

By differentiating (3.20) and (3.21), voltages are decoupled from currents, as given by

$$\frac{\mathrm{d}^2}{\mathrm{d}z^2}\mathbf{v}(z) = \mathbf{Z}\mathbf{Y}\mathbf{v}(z) \tag{3.22}$$

$$\frac{\mathrm{d}^2}{\mathrm{d}z^2}\mathbf{i}(z) = \mathbf{Y}\mathbf{Z}\mathbf{i}(z) \tag{3.23}$$

However, the voltages and currents are still coupled by themselves. Eigenvalue decomposition is applied to decouple the voltages and currents, as expressed by

$$\mathbf{T}_V^{-1}\mathbf{Z}\mathbf{Y}\mathbf{T}_V = \mathbf{\Lambda} \tag{3.24}$$

$$\mathbf{T}_I^{-1}\mathbf{Y}\mathbf{Z}\mathbf{T}_I = \mathbf{\Lambda} \tag{3.25}$$

where the columns of $\mathbf{T}_V$ and $\mathbf{T}_I$ are eigenvectors and the diagonal of $\mathbf{\Lambda}$ contains eigenvalues λ_i^2. If $\mathbf{Z}$ and $\mathbf{Y}$ are symmetric, $\mathbf{T}_V$ and $\mathbf{T}_I$ are the same. The decoupled voltages and currents are defined as mode voltages $\mathbf{v}_m(z)$ and mode currents $\mathbf{i}_m(z)$, as given by

$$\mathbf{v}(z) = \mathbf{T}_V\mathbf{v}_m(z) \tag{3.26}$$

$$\mathbf{i}(z) = \mathbf{T}_I\mathbf{i}_m(z) \tag{3.27}$$

$\mathbf{T}_V$ and $\mathbf{T}_I$ define a transformation between the actual line voltages and currents and the mode voltages and currents. Substituting (3.26) and (3.27) into (3.22) and (3.23) yields

$$\frac{\mathrm{d}^2}{\mathrm{d}z^2}\mathbf{v}_m(z) = \mathbf{T}_V^{-1}\mathbf{Z}\mathbf{Y}\mathbf{T}_V\mathbf{v}_m(z) = \mathbf{\Lambda}\mathbf{v}_m(z) \tag{3.28}$$

$$\frac{\mathrm{d}^2}{\mathrm{d}z^2}\mathbf{i}_m(z) = \mathbf{T}_I^{-1}\mathbf{Y}\mathbf{Z}\mathbf{T}_I\mathbf{i}_m(z) = \mathbf{\Lambda}\mathbf{i}_m(z) \tag{3.29}$$

The mode voltages and currents are now decoupled and they can be expressed as

$$\mathbf{v}_m(z) = \mathbf{e}^{-\sqrt{\Lambda}z}\mathbf{v}_m^+ + \mathbf{e}^{\sqrt{\Lambda}z}\mathbf{v}_m^- \tag{3.30}$$

$$\mathbf{i}_m(z) = \mathbf{e}^{-\sqrt{\Lambda}z}\mathbf{i}_m^+ - \mathbf{e}^{\sqrt{\Lambda}z}\mathbf{i}_m^- \tag{3.31}$$

where the matrix exponentials are defined as $\mathbf{e}^{\pm\sqrt{\Lambda}z} = \mathcal{D}([e^{\pm\lambda_0 z}, \ldots, e^{\pm\lambda_{n-1}z}])$, $\mathbf{v}_m^{\pm}$ and $\mathbf{i}_m^{\pm}$ are $n \times 1$ vectors of undetermined constants associated with the forward/backward-travelling waves of modes. From here it can be concluded that signals do not propagate in individual conductors separately. Instead, they propagate across conductors in the form of modes. Different modes can propagation at the same time independently. However, mode voltages and currents cannot be measured. They can only be obtained from the above conversion once the line voltages and currents are measured.

The line voltages and currents are now expressed by

$$\mathbf{v}(z) = \mathbf{Z}_C\mathbf{T}_I(\mathbf{e}^{-\sqrt{\Lambda}z}\mathbf{i}_m^+ + \mathbf{e}^{\sqrt{\Lambda}z}\mathbf{i}_m^-) \tag{3.32}$$

$$\mathbf{i}(z) = \mathbf{T}_I(\mathbf{e}^{-\sqrt{\Lambda}z}\mathbf{i}_m^+ - \mathbf{e}^{\sqrt{\Lambda}z}\mathbf{i}_m^-) \tag{3.33}$$

where $\mathbf{Z}_C = \mathbf{Y}^{-1}\mathbf{T}_I\sqrt{\mathbf{\Lambda}}\mathbf{T}_I^{-1}$ is defined as the characteristic impedance of the transmission line. Incorporating terminal conditions

$$\mathbf{v}(0) = \mathbf{v}_S - \mathbf{Z}_S\mathbf{i}(0) \tag{3.34}$$

$$\mathbf{v}(\mathscr{L}) = \mathbf{v}_L - \mathbf{Z}_L\mathbf{i}(\mathscr{L}) \tag{3.35}$$

where $\mathbf{v}_S$ and $\mathbf{Z}_S$ are source voltage and impedance, $\mathbf{v}_L$ is the load voltage bias and it is usually set to zero, $\mathbf{Z}_L$ is the load impedance matrix. The forward/backward-travelling current waves can be obtained from solving

$$\begin{bmatrix} (\mathbf{Z}_C + \mathbf{Z}_S)\mathbf{T}_I & (\mathbf{Z}_C - \mathbf{Z}_S)\mathbf{T}_I \\ (\mathbf{Z}_C - \mathbf{Z}_L)\mathbf{T}_I\mathbf{e}^{-\sqrt{\Lambda}\mathscr{L}} & (\mathbf{Z}_C + \mathbf{Z}_L)\mathbf{T}_I\mathbf{e}^{\sqrt{\Lambda}\mathscr{L}} \end{bmatrix} \begin{bmatrix} \mathbf{i}_m^+ \\ \mathbf{i}_m^- \end{bmatrix} = \begin{bmatrix} \mathbf{v}_S \\ \mathbf{v}_L \end{bmatrix} \tag{3.36}$$

$\mathbf{v}(0)$ and $\mathbf{v}(\mathscr{L})$ then can be obtained by substituting $\mathbf{i}_m^{\pm}$ into (3.32). The transmission line transfer function is then given by

$$\begin{aligned} \mathbf{H}_0(f) &= \mathbf{v}(\mathscr{L})\mathbf{v}(0)^{-1} \\ &= \mathbf{Z}_C\mathbf{T}_I(\mathbf{I}_n - \rho_{LI})(\mathbf{e}^{-\sqrt{\Lambda}\mathscr{L}} - \mathbf{e}^{\sqrt{\Lambda}\mathscr{L}}\rho_{LI})^{-1}\mathbf{T}_I^{-1}\mathbf{Y}_C \end{aligned} \tag{3.37}$$

where $\mathbf{I}_n$ is an $n \times n$ identity matrix, $\mathbf{Y}_C = \mathbf{Z}_C^{-1}$ is the characteristic admittance, ρ_{LI} is the current reflection coefficient at load, as expressed by

$$\rho_{LI} = \mathbf{T}_T^{-1}\mathbf{Y}_C(\mathbf{Y}_L + \mathbf{Y}_C)^{-1}(\mathbf{Y}_L - \mathbf{Y}_C)\mathbf{Z}_C\mathbf{T}_I \tag{3.38}$$

where $\mathbf{Y}_L = \mathbf{Z}_L^{-1}$ is the load admittance. To obtain the overall channel transfer function, $\mathbf{H}_S(f) = \mathbf{v}(0)\mathbf{v}_S^{-1}$ is required. The computation is a bit tricky because $\mathbf{v}_S$ is a vector and it has no inverse. To solve the problem, we build a matrix $\mathcal{V}_S = [\mathbf{v}_{S1}, \ldots, \mathbf{v}_{SK}]$ in which $\mathbf{v}_{Sk}$ is a set of arbitrarily chosen orthogonal vectors and $K \geq n$. Then the overall channel transfer function is given by

$$\mathbf{H}(f) = \mathbf{H}_0(f)\mathbf{v}(0)\mathcal{V}_S^{\dagger} \tag{3.39}$$

where $\mathcal{V}_S^{\dagger}$ is the pseudo-inverse of $\mathcal{V}_S$. Finally, the input admittance at source is given by

$$\mathbf{Y}_{in}(0) = \mathbf{T}_I(\mathbf{I}_n + \rho_{LI})(\mathbf{I}_n - \rho_{LI})^{-1}\mathbf{T}_I^{-1}\mathbf{Y}_C \tag{3.40}$$

This is required when calculating the transfer function of a network.

MTL theory can be used to study MIMO PLC. When a set of input signals $\mathbf{v}_S$ are applied to one end of a transmission line, they are virtually converted to mode voltages and then propagate through the transmission line independently. At the load, they are converted back to line voltages and the measured line voltages are mixtures of the transmitted signals. If the transformation between line voltages and mode voltages are known, the transmitted signals can be easily separated. However, life is always hard. Although the transformation can be obtained by analysing the transmission line, there are some mechanisms in the network that will destroy the independence between mode voltages. For example, if the load impedance matrix is not diagonal, the reflected signals will be mixed. In fact, our investigation has shown that the only way to figure out the overall coupling between signals is through channel estimation, like what is done in wireless communication.

3.2.3 Transfer Function Computation

The voltage ratio approach is an efficient solution to channel transfer function computation. The basic idea is to divide the power network between the transmitter and the receiver into a number of segments and the overall transfer function is the product of the transfer functions of the segments. This approach is demonstrated using the 2TL theory in this section.

To use the approach, first, the backbone, which is the shortest path between the transmitter and the receiver, is identified. Then, along the backbone, the network is broken into multiple pieces. The breakpoints are chosen arbitrarily but for convenience we suggest to break the network at the points where branches are attached to the backbone, as illustrated in Fig. 3.5. We denote the transfer function of each segment as $H_n(f) = V_{n+1}(f)/V_n(f)$. The overall transfer function is then written as

$$H(f) = \frac{V_{N+1}(f)}{V_1(f)} = \prod_{n=1}^{N} H_n(f) \tag{3.41}$$

Note that this equation is adopted in [12] and it assumes source impedance is zero hence $V_1(f) = V_S(f)$. Considering the source impedance, the overall channel transfer function can be written as

$$H_S(f) = \frac{V_2(f)}{V_S(f)}\frac{V_{N+1}(f)}{V_2(f)} = \frac{V_1(f)}{V_S(f)}\frac{V_{N+1}(f)}{V_1(f)} \tag{3.42}$$

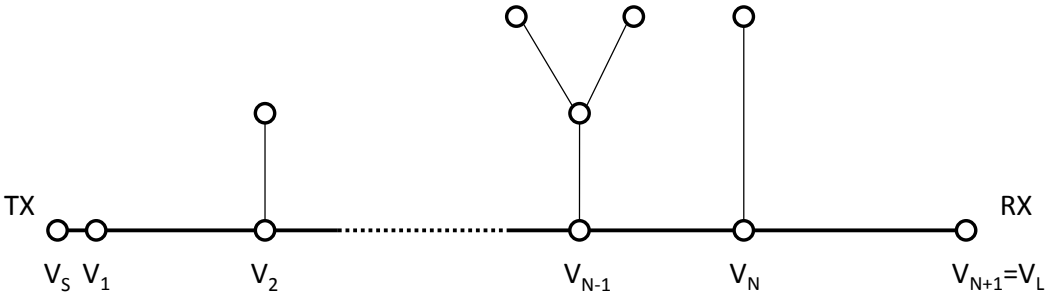

Fig. 3.5: Illustration of network segmentation

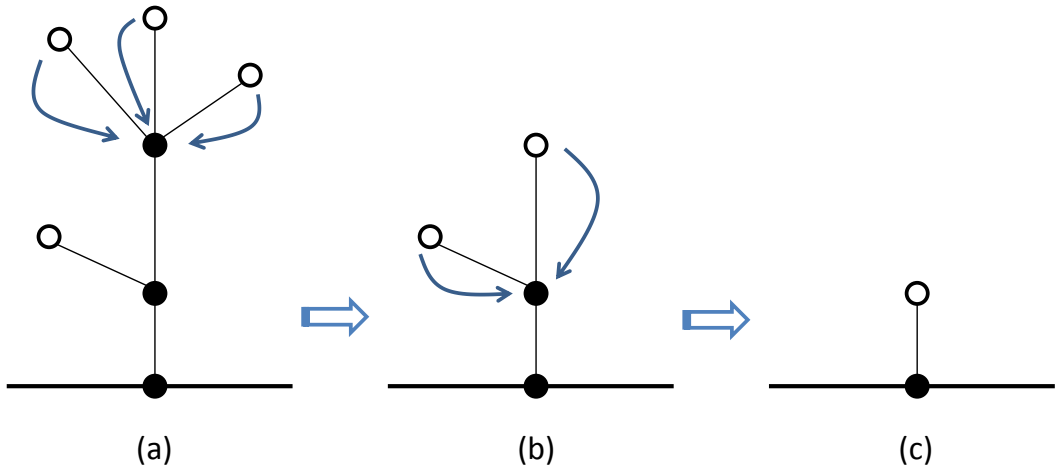

Fig. 3.6: Illustration of impedance carry back

In this equation we provide two implementation options. One is to use (3.19) to calculate $V_2(f)/V_S(f)$. The other one is to calculate $V_1(f)/V_S(f)$ with

$$\frac{V_1(f)}{V_S(f)} = \frac{V(0)}{V_S} = \frac{1+\Gamma_L e^{-2\gamma\mathscr{L}}}{1-\Gamma_S\Gamma_L e^{-2\gamma\mathscr{L}}}\frac{Z_C}{Z_C+Z_S} \tag{3.43}$$

Except for the calculation of the transfer function of the segment that is connected to the source, all the other transfer functions can be calculated with (3.18). To use this equation, the line propagation constant, line length and load impedance is required. It is important to note that the load impedance of segment n is in fact the input impedance of segment $n+1$. The calculation of the input impedance of segment $n+1$ requires the method called impedance carry back [12] because the effective input impedance considers the backward-travelling wave reflected back from the receiver so that the receiver impedance needs to be "carried back" to the point of interest. The effect of branches can also be processed with this method. No matter how complex a branch is, it can be represented by a single impedance. This is illustrated in Fig. 3.6.

An example: the T-shaped network

Here we use the simplest network, the T-shaped network, to demonstrate the steps of using the impedance carry back method and the voltage ratio approach to calculate the channel transfer function. The network is shown in Fig. 3.7 and all the required network elements are labelled. In this figure, thick lines represent transmission lines with the same characteristic impedance Z_C and propagation constant γ while thin lines represent negligible connection wires. The lengths of the two segments of lines and the branch are l_1, l_2 and l_{Br}, respectively.

The first step is to calculate the transfer function of the segment BC, which is given by

$$H_{BC}(f) = \frac{1 + \Gamma_L}{e^{\gamma l_2} + \Gamma_L e^{-\gamma l_2}}$$

where $\Gamma_L = (Z_L - Z_C)/(Z_L + Z_C)$. The next step is to calculate the effective input impedance looking into node B. The input impedances of the branch and the segment BC are written as

$$Z_{Br}^{(in)} = Z_C \frac{1 + \Gamma_{Br} e^{-2\gamma l_{Br}}}{1 - \Gamma_{Br} e^{-2\gamma l_{Br}}}$$
$$Z_{BC}^{(in)} = Z_C \frac{1 + \Gamma_L e^{-2\gamma l_2}}{1 - \Gamma_L e^{-2\gamma l_2}}$$

where $\Gamma_{Br} = (Z_{Br} - Z_C)/(Z_{Br} + Z_C)$. Since the combination of the branch and the segment BC can be seen as a parallel circuit, the effective input impedance is expressed as

$$Z_B^{(in)} = \frac{Z_{Br}^{(in)} Z_{BC}^{(in)}}{Z_{Br}^{(in)} + Z_{BC}^{(in)}}$$

Now we can calculate the transfer function of the segment AB, as expressed by

$$H_{AB}(f) = \frac{1 + \Gamma_B}{e^{\gamma l_1} + \Gamma_B e^{-\gamma l_1}}$$

where $\Gamma_B = (Z_B^{(in)} - Z_C)/(Z_B^{(in)} + Z_C)$. Finally, using (3.43), the overall transfer function is given by

$$H_S(f) = \frac{1 + \Gamma_B e^{-2\gamma l_1}}{1 - \Gamma_S \Gamma_B e^{-2\gamma l_1}} \frac{Z_C}{Z_C + Z_S} H_{AB}(f) H_{BC}(f)$$

where $\Gamma_S = (Z_S - Z_C)/(Z_S + Z_C)$.

3.3 A Linear Periodic Time-Varying Channel Model

According to [9], the indoor power line channel can be approximated as a periodic time-varying linear filter. The variation is synchronous to alternating current (AC)

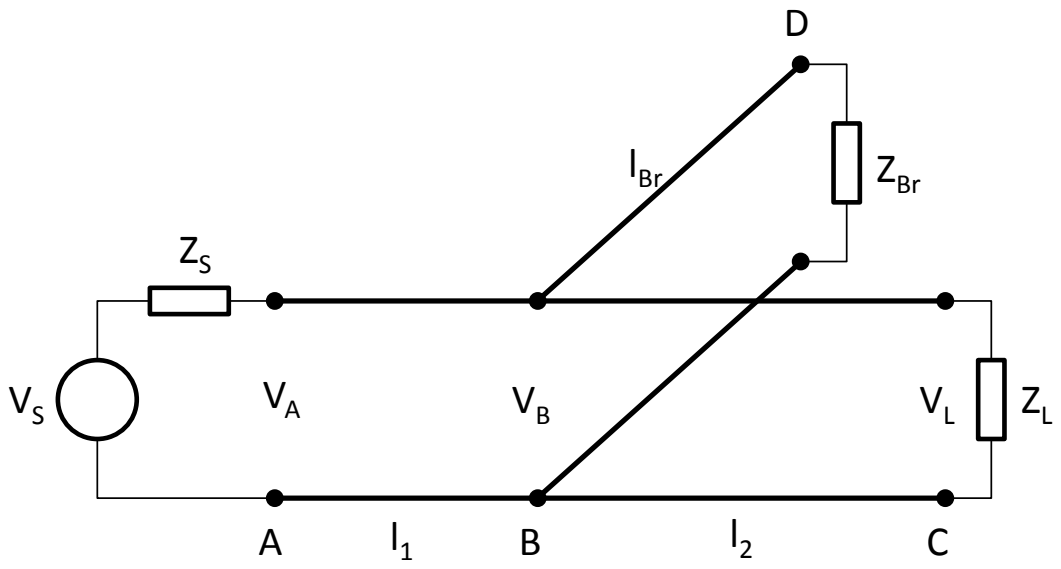

Fig. 3.7: The T-shaped network

power supply and has a frequency that is twice of the AC frequency (e.g. 100 Hz if AC frequency is 50 Hz). This is because the impedances of some appliances in the network response to AC sinusoidal variation. These appliances usually contain motors or rectify circuits. The work also shows that the channel can be seen as approximately time-invariant provided that the interval is shorter than the coherence time. Therefore, to model the channel, we use a number of time-invariant linear filters and the coefficients of each filter are determined by assuming the channel does not change during that interval. In frequency domain the filtering can be expressed as

$$Y(f) \approx H(t,f)|_{t=t_0} X(f) \tag{3.44}$$

where $Y(f)$ and $X(f)$ are the output signal and input signal, respectively, t_0 is the time instant at which the signal is transmitted, $H(t,f)$ is the time-varying channel transfer function with $H(t,f) = H(t+T_0/2,f)$ and T_0 is the mains period.

In this section we explain the linear periodic time-varying (LPTV) channel model that is adopted in this thesis. This model is a combination of the 2TL theory and the LPTV channel model proposed in [5]. We use the voltage ratio approach for channel transfer function generation. The channel model is then made time-varying by introducing the time-varying load models proposed in [5]. Therefore, in this section we mainly introduce how a time-varying power network is composed. This includes a network topology, time-varying load models and cable parameters. Based on this model, we develop a simulation tool that is able to generate random channel realisations. Some key issues related to this tool is explained.

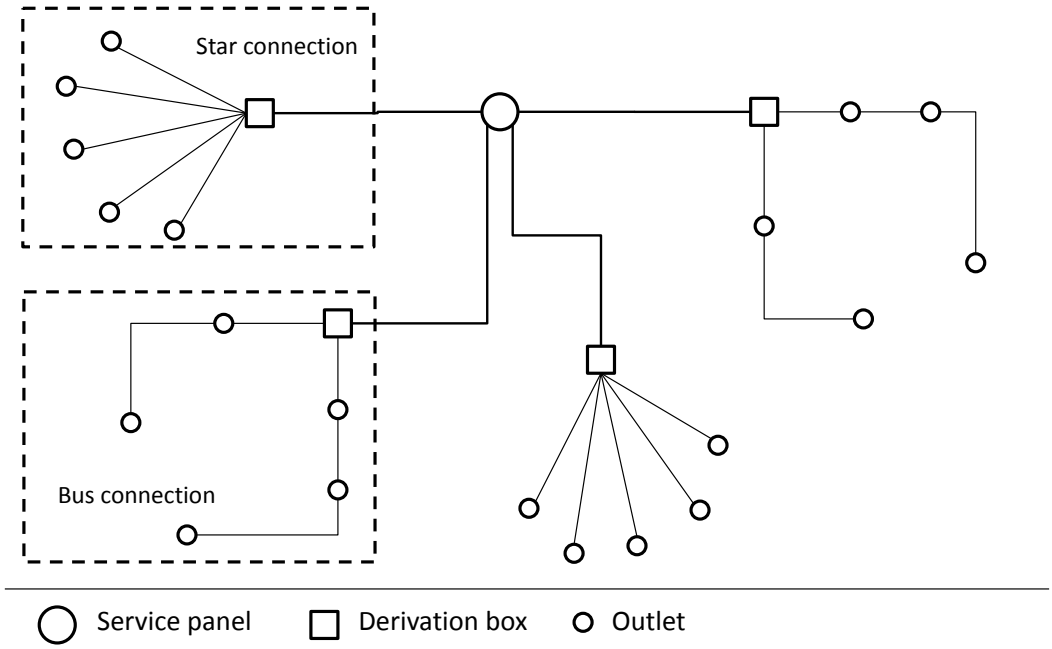

Fig. 3.8: An example of indoor power network topology

3.3.1 Indoor Power Network Topology

Indoor power network usually has a two-level tree structure [12, 37] as shown in Fig. 3.8. In the first level, the power is distributed from the service panel to a number of derivation boxes. The number of derivation boxes depends on the house layout. A few outlets are connected to each derivation box. The connection can be either in star type or in bus type. In [12] an algorithm is developed to generate such kind of topologies randomly. In simulation, derivation boxes and the service panel are treated as intermediate nodes that do not affect the channel transfer function. Each outlet can be connected to a load or left open. The channel transfer function between any two outlets can be calculated with a bottom-up model as long as a signal source and a sink are connected to the corresponding outlets.

In this thesis, we use the simplified topology proposed in [5] because it is simple and accurate enough for simulation. This topology is shown in Fig. 3.9. Except for the signal source and sink, there are three branches as well as three loads connected to the main line between source and sink. There are seven line segments including the three branches and the four main line segments separated by the branches. The choice of the length of line segments, loads and cables will be given in section 3.3.4.

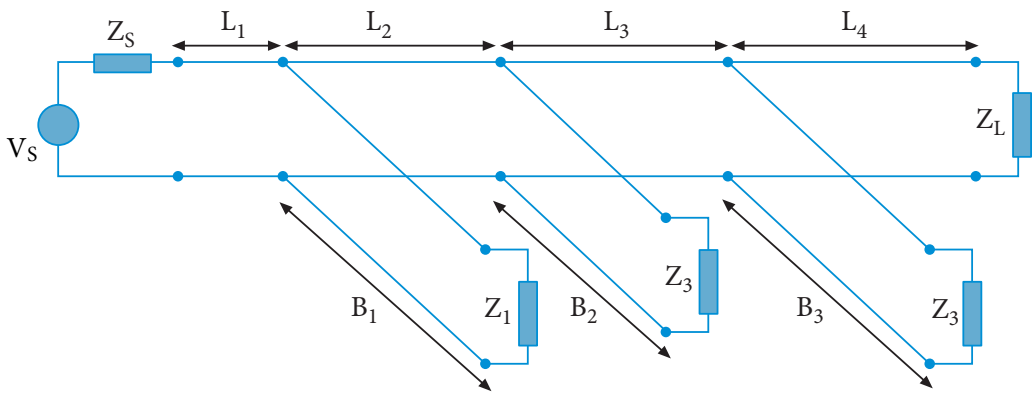

Fig. 3.9: A simplified indoor power network topology [5]

3.3.2 Load Models

According to [5], the loads in an indoor power network can be classified into three groups, namely constant impedances, frequency-selective impedances and time-varying impedances.

Constant impedances are approximately constant in time and frequency. This is, in practice, not a common case. Typical values are $\{5, 50, 150, 1000, \infty\}\Omega$, representing low, radio frequency (RF) standard, matched-to-transmission-line Z_C, high, and open circuit impedances.

Frequency-selective (time-invariant) impedances are modelled by parallel RLC resonant circuits, as expressed by

$$Z(\omega) = \frac{R}{1 + jQ\left(\frac{\omega}{\omega_0} - \frac{\omega_0}{\omega}\right)} \tag{3.45}$$

where R is the resistance at resonant frequency, ω_0 is angular resonant frequency, ω is angular frequency and Q is called quality factor that determines the frequency selectivity of the impedance.

Time-varying impedances are frequency-selective as well. They can be divided into two classes of behaviours. One of them is named commuted behaviour which describes the impedance switching between two distinct values Z_A and Z_B. This is illustrated in Fig. 3.10. As stated above, the variation is synchronous to the AC power wave and has a period that is half of the mains period T_0. In addition, the impedance variation has a state duration of T and it may have a delay of D with respect to the mains voltage zero-crossing. The other behaviour corresponds to a more "harmonic" impedance variation that can be modelled with an absolute sinusoidal function, as expressed by

$$Z(\omega, t) = Z_A(\omega) + Z_B(\omega)\left|\sin\left(\frac{2\pi}{T_0}t + \phi\right)\right| \tag{3.46}$$

where Z_A and Z_B are the offset impedance and the amplitude of the impedance respectively, and it also has a phase shift ϕ with respect to the voltage zero-crossing.

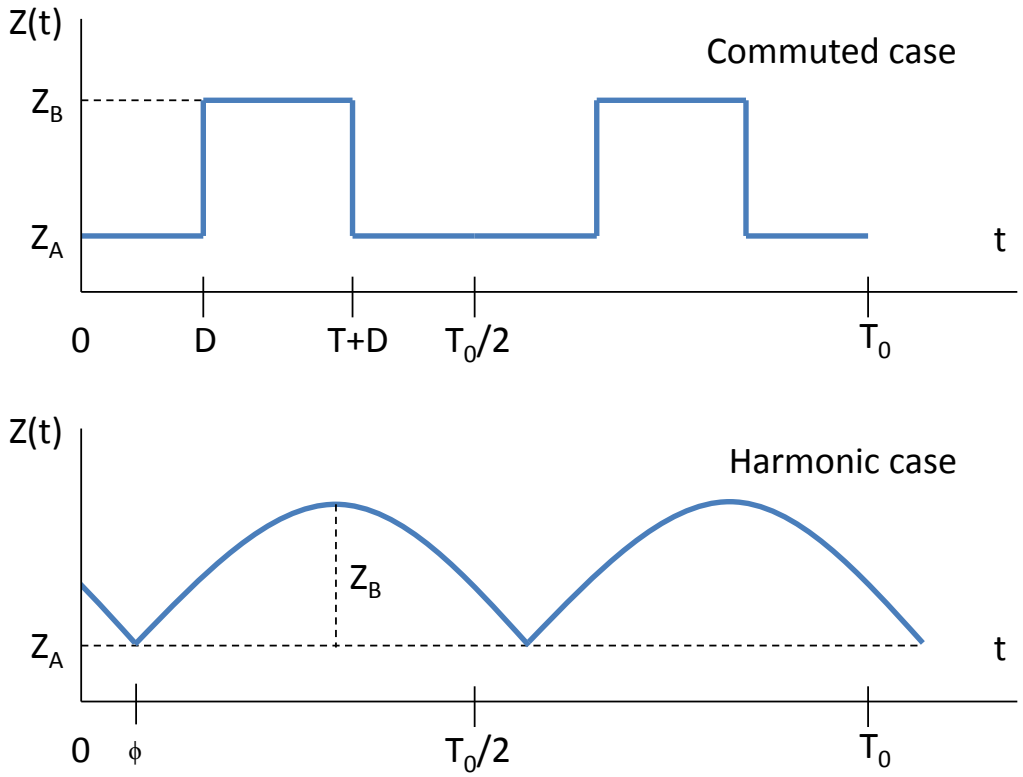

Fig. 3.10: Illustration of time-varying impedances: the commuted case and the harmonic case

3.3.3 Transmission Line Parameters

Knowledge of the four basic p.u.l parameters is of paramount importance to the calculation of transfer functions. For some simple and idea transmission lines with symmetric cross-sections, closed form solutions can be found with respect to the geometry of the transmission line cross-section. This topic has been well studied in the subject of EM engineering, such as in [39, 40] and chapter 4 of [4].

On the contrary, for some complex transmission lines with asymmetric cross-sections, complex numerical methods have to be used [34]. Even so, such kind of theoretical models are not accurate enough because in practice most of the idea situations cannot be met and uncertainties always present. Therefore, the best solution to find out p.u.l parameters is through measurement. It is important to point out that according to the work of Sartenaer [34] once the models of the transmission lines used in a network are verified with measurements, it is not necessary to verify the model of the whole network. This proves the validity and accuracy of a bottom-up approach.

In this thesis, we use the p.u.l parameters obtained by the measurement work of Cañete, as presented in [5] and Table 3.1. Five kinds of typical indoor transmission lines are given. It should be noted that the characteristic impedance Z_C, the p.u.l capacitance C and inductance L are approximately constant in frequency. The p.u.l resistance

Table 3.1: Characteristics of practical indoor power lines

Cable type	0	1	2	3	4
$Z_C(\Omega)$	270	234	209	178	143
C(pF/m)	15	17.5	20	25	33
L(μH/m)	1.08	0.96	0.87	0.78	0.68
R_0	12	9.34	7.55	6.25	4.98
G_0	30.9	34.7	38.4	42.5	49.3

R and conductance G are frequency dependent and are given by $R = R_0\sqrt{f}\cdot 10^{-5}(\Omega/m)$ and $G = 2\pi f G_0 l \cdot 10^{-14}(S/m)$, where l is used to compensate the attenuation loss due to the simplified network topology.

3.3.4 Implementation and Simulation Results

In this section we present the implementation of the LPTV model based simulation tool and a sample channel realisation generated using this tool.

Parameters Setup

We first introduce some criteria to set up proper values for the parameters required for simulation.

1. The transmitter and receiver have constant impedance of 50Ω;
2. One type of transmission line, chosen from Table 3.1 randomly with uniform distribution, is used throughout the whole network (i.e. no mixture of different cables);
3. Line segment lengths are chosen randomly between 0.5 and 50 m with uniform distribution;
4. Constant impedances are randomly chosen from $\{5, 50, 150, 1000, \infty\}\Omega$ with a uniform distribution;
5. Frequency selective impedances are obtained by choosing the following parameters randomly:
   (a) Resistance at resonance is chosen from $\{200, 1800\}\Omega$ with a uniform distribution;
   (b) Resonant frequency is chosen from $\{3, 200\}$kHz with a uniform distribution;
   (c) The Q factor is chosen from $\{5, 25\}$ with a uniform distribution.
6. At least one of the three loads in Fig. 3.9 should be a time-varying load. In the case of a commuted load, the following parameters apply:
   (a) Z_B is chosen in the same way as a frequency-selective impedance;
   (b) $Z_A = Z_B \cdot 0.5$;

(c) Suppose the channel is divided into M invariant intervals according to its coherence time (e.g. 400 ms [5]), the duration T in discrete time, is chosen between 1 and $M/4$ uniformly;
(d) Delay D is chosen from $\{0, M/2 - T\}$ uniformly.

In the case of a harmonic load, the parameters would be:

(a) Z_B is also a frequency-selective impedance;
(b) Z_A is fixed at 5Ω;
(c) The phase ϕ is chosen uniformly between 0 and π rad.

These are the general rules for setting up the parameters. Specifically, in our simulation, we use two frequency-selective loads and one harmonic load. Besides, the mains AC frequency is 50 Hz.

Implementation

The general steps of channel transfer function generation are summarised as follows:

1. The network topology is defined with randomly chosen cable lengths;
2. One type of cable is randomly chosen from the database;
3. Several loads are randomly generated according to the time-varying load models;
4. The channel transfer function is computed.

Within these steps, the definition of network topology is of paramount importance to channel transfer function computation. In addition, the impedance carry back method used in transfer function calculation is the most challenging part. Therefore, we focus on these two issues in this section.

First of all, the topology is described by an adjacency matrix $\mathbf{A}$. If nodes n and m are connected by a transmission line of length l_{nm}, we have $[\mathbf{A}]_{n,m} = [\mathbf{A}]_{m,n} = l_{nm}$, otherwise, $[\mathbf{A}]_{n,m} = [\mathbf{A}]_{m,n} = 0$. The vector $[\mathbf{A}]_n$ then indicates the nodes that are connected to node n. The adjacency matrix is originally used in graph theory to describe a graph. Hence, by adopting the algorithms developed in graph theory, we can find the shortest path (the backbone) between any two nodes.

Recursive programming is adopted for the implementation of impedance carry back. As stated above, the calculation of the input impedance at an intermediate node requires the impedances seen at its adjacent nodes, which in turn requires the calculation of the input impedances of those adjacent nodes. This is a recursive process and is better to be realised with recursive programming. The algorithm is described in Algorithm 1. For convenience, we use "lineInputImped" to represent a function that calculates the input impedance of a line segment nm using (3.15). This function has an argument which is the load impedance connected to the line segment nm. The implementation of voltage ratio approach is straightforward hence it is not presented here.

Algorithm 1 A recursive function that implements impedance carry back

```
function INPUTIMPEDANCE(A,n)
    adjNodes = [A]_n                                  ▷ get adjacent nodes
    adjNodes = adjNodes - (n − 1)                     ▷ node n − 1 should not be considered
    inputImped = Inf                                  ▷ initialise input impedance to infinity
    for m = adjNodes do                               ▷ for each node in adjNodes
        if node m is an outlet then
            z = outlet load impedance
            tempImped = LINEINPUTIMPED(z)
        else
            inputImped_m = INPUTIMPEDANCE(A,m)        ▷ call the function itself
            tempImped = LINEINPUTIMPED(inputImped_m)
        end if
        inputImped = 1/(1/inputImped+1/tempImped)
    end for
    return inputImped
end function
```

Extending to MTLs

The developed power line channel simulation tool can be easily extended to generating MTL-based power line networks since the voltage ratio approach and the impedance carry back method is independent of the number of conductors in a transmission line. The major changes that should be conducted are summarised as follows. First of all, the whole system or programme should be able to deal with voltage and current vectors instead of scalars. In addition, p.u.l parameters and load impedances are now in the form of matrices. Second, equations 3.37 through 3.40 should be used for the calculation of transfer functions, reflection coefficients and input impedances. Finally, a simple voltage conversion should be added in order to support not only MIMO PLC but also single-input-multiple-output (SIMO) and multiple-input-single-output (MISO) PLC. This conversion can be found in [33].

Simulation Results

The upper figure of Fig. 3.11 shows a typical LPTV indoor power line channel realisation that is generated using the model described above. The channel varies in a period of about 10 ms as the mains period is 20 ms. Frequency-selectivity and time-selectivity can be observed clearly. It can be seen that the channel varies fast at its rising and falling edge while it is quite flat in between. In the bottom figure we plot the subcarrier averaged signal-to-interference ratio (SIR) of an OFDM block transmitted in different intervals of the channel. It is clear that signal transmitted at rising or falling edge of each cycle suffers from low SIR. This is because channel variation induces power leakage from one subcarrier to its adjacent ones causing the so-called ICI. This increases interference power while reduces signal power. SIR less than 20 dB can be regarded as

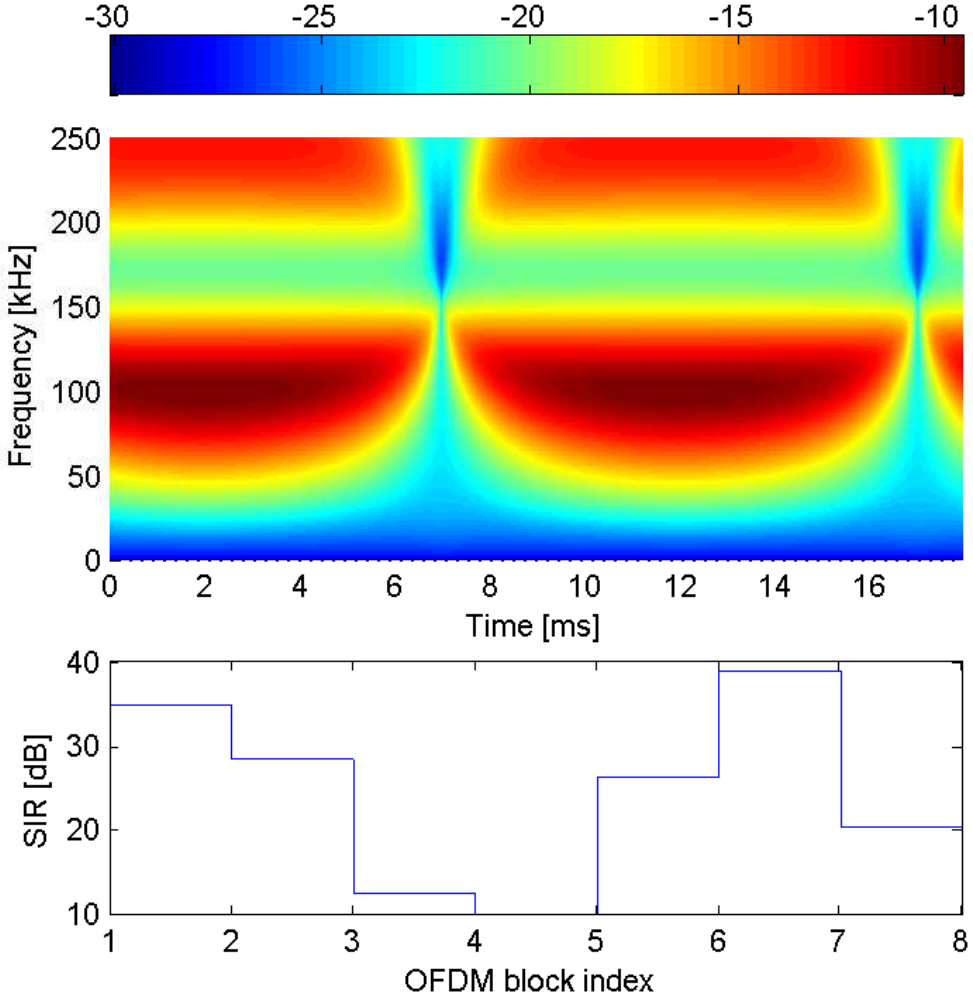

Fig. 3.11: Up: a typical LPTV power line channel realisation; bottom: subcarrier averaged SIR of an OFDM block transmitted in different intervals of the above channel

dangerous because in this case interference may be more significant than noise.

In Fig. 3.12 we show the frequency response of a 2-by-2 MIMO power line channel generated with the extended simulation tool. Since there is no time-varying load models which support MTLs, a time-fixed channel realisation is shown. This figure was generated with the power network topology in Fig. 3.7 with $l_1 = 5.22m$, $l_2 = 3.60m$ and $l_{Br} = 2.30m$. The source impedance Z_S, load impedance Z_L and branch load impedance Z_{Br} are all the same, equal to

$$Z = \begin{bmatrix} 50 & 0 \\ 0 & 50 \end{bmatrix} \Omega \tag{3.47}$$

The MTL used in this simulation is a symmetric three-conductor transmission line. The structure and p.u.l parameters can be found in [33].

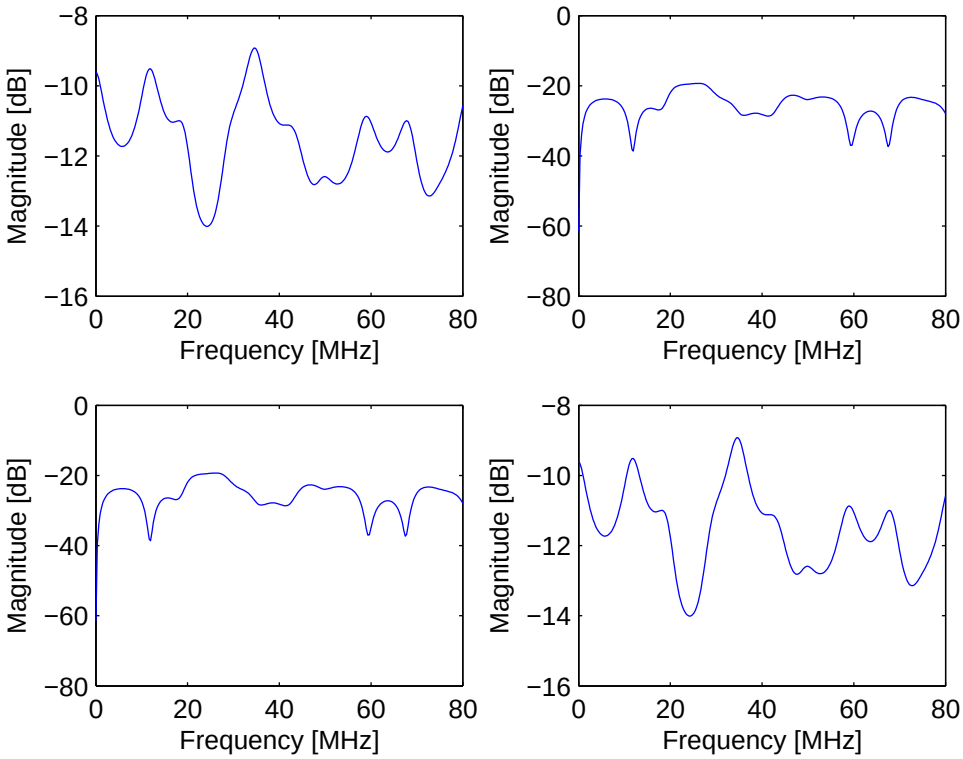

Fig. 3.12: Frequency response of a 2-by-2 MIMO power line channel

Since two closed circuits can be formed with a three-conductor transmission line, the channel has two inputs and two outputs. In Fig. 3.12, the two plots on the main diagonal show the desired the channel responses which are the responses of the channel between input i and output i. On the other hand, the other two plots show the coupled channel responses between input i and output j. Because everything in the network, including the transmission line and all the loads, are symmetric, the resultant channel responses are also symmetric. In this case, mode voltages and currents can be obtained easily using the aforementioned eigenvector conversion. However, if anything in the network is asymmetric, the channel will no longer be symmetric and mode voltages and currents will be hard to obtain.

3.4 Noise Models

Since power grid is a bus system, noise or interference generated in the network, no matter where it is, may be sensed by the receiver. In an indoor power network, the noise generated by appliances is filtered by the channel and then superimposed at the receiver [41], causing a compound noise scenario that consists coloured background noise and complex impulsive noise. Coloured background noise is caused by superposition of low-pass filtered noise sources. As a result, the noise at receiver has a power spectral density

(PSD) that decays fast as frequency increases. Impulsive noise is caused by different kinds of switching events occur in the network, such as the switching mechanism in power supplies and artificial switching controls. Different kinds of impulsive noise can be observed at the receiver [42]. They are periodic impulsive noise synchronous with the mains frequency, periodic impulsive noise asynchronous with the mains frequency and aperiodic impulsive noise. Periodic impulsive noise usually has a constant power and its period is determined by the specific circuit design of a power supply device. Aperiodic impulsive noise is random and may be caused by multiple switching events. In addition to coloured background noise and impulsive noise, transmission lines may pick up unwanted low-frequency through high-frequency radio signals. Such an interference is regarded as narrowband noise/interference in literature.

In this section we introduce some representative impulsive noise models and coloured background noise PSD. We will also introduce a cyclostationary noise model that is developed for time-varying power line channels. Narrowband interference is not considered in this thesis.

3.4.1 Coloured Background Noise

Coloured background noise is usually assumed to be Gaussian and its PSD is obtained by measurements and data fitting. Different fitting curves can be found in literature [6, 31, 43] but with properly estimated parameters, they give similar results.

In the first model [31], noise PSD is assumed to be

$$S(f) = a + b|f|^c \ dBm/Hz \tag{3.48}$$

where in the worst case $a = -145$, $b = 53.230$ and $c = -0.337$ and in the best case $a = -140$,$b = 38.75$ and $c = -0.72$. Note that f is in the unit of MHz.

In the second model [43] noise PSD is written as

$$S(f) = A_\infty + A_0 e^{-f/f_0} \ dB/Hz \tag{3.49}$$

where two sets of parameters are provided, they are $A_\infty = -136$, $A_0 = 38$ and $f_0 = 0.7$, and $A_\infty = -140$, $A_0 = 75$ and $f_0 = 0.5$. Similarly, f and f_0 are in the unit of MHz.

The third model is relatively simple, as expressed by

$$S(f) = \frac{a}{2} e^{-a|f|} \tag{3.50}$$

where $a = 1.2e - 5$. It should be noted that the first two models are in dB or dBm scale while the third model is in linear scale. A comparison of these models is plotted in Fig. 3.13 with a focus on the low-frequency region. Since the first and the second model are obtained from measurements conducted in MHz region, they present similar and reasonable PSD in this region. However, it should be noted that noise power in the first model is not bounded. The third model is only valid in the kHz region due

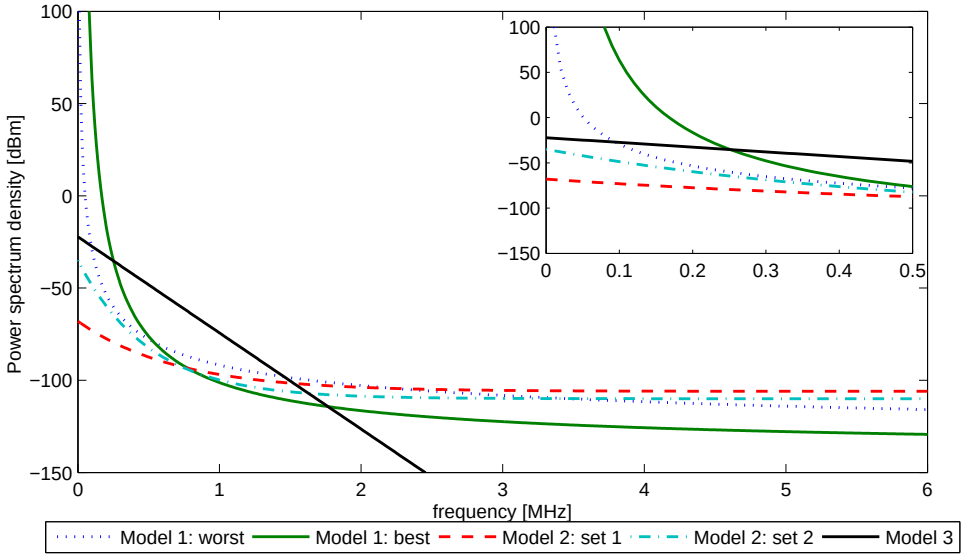

Fig. 3.13: A comparison of noise PSD models

to measurement limitation. Among these models, the second model seems to be the best one because it provides reasonable values when frequency is very low or very high. Despite these differences, all these curves show that NB-PLC systems should expect a high noise power.

3.4.2 Impulsive Noise

This section introduces some representative random impulsive noise models. The study of periodic impulsive noise is not popular in literature. [3] proposes to use a pulse train to switch on and off impulsive noise periodically. There are three popular random impulsive models in literature, namely the Middleton's class A model [44], the Bernoulli Gaussian model [45] and the Markov chain model [42].

The Middleton's class A model is a kind of infinite Gaussian mixture model whose probability density function (pdf) is expressed by

$$p_\eta(v) = \sum_{k=0}^{\infty} w_k \mathcal{N}(0, \sigma_k^2) \tag{3.51}$$

where $w_k = e^{-A} A^k / k!$ is the Poisson distribution that controls the occurrence of impulsive noise components and $\sum_{k=0}^{\infty} w_k = 1$, A is called the impulsive index, $\mathcal{N}(0, \sigma_k^2)$ represents a Gaussian distribution with zero mean and variance σ_k^2 and

$$\sigma_k^2 = \left(\frac{k/A + \Delta}{1 + \Delta} \right) (\sigma_b^2 + \sigma_i^2) = \sigma_i^2 \frac{k}{A} + \sigma_b^2 = \left(\frac{1}{\Delta} \frac{k}{A} + 1 \right) \sigma_b^2 \tag{3.52}$$

where $\Delta = \sigma_b^2 / \sigma_i^2$ is the ratio of background noise power to impulsive noise power. From the distribution in (3.51) we can see that high power impulsive noise is very rare.

Therefore, this model is usually approximated with the first three terms of (3.51), as expressed by

$$p_\eta(\upsilon) \approx w_0\mathcal{N}(0,\sigma_0^2) + w_1\mathcal{N}(0,\sigma_1^2) + w_2\mathcal{N}(0,\sigma_2^2) \tag{3.53}$$

The Bernoulli Gaussian model is in fact a further simplified version of Middleton's class A model because it is a mixture of only two Gaussian distributions, as expressed by

$$p_\eta(\upsilon) = (1-P)\mathcal{N}(0,\sigma_b^2) + P\mathcal{N}(0,K\sigma_b^2) \tag{3.54}$$

where P is the probability of impulsive noise occurrence and K is the ratio of impulsive noise power to background noise power. It should be noted that the K here is different from the $1/\Delta$ of the Middleton's model.

The Markov chain model is the most complex but perhaps the most accurate impulsive noise model. Zimmermann's Markov chain model [42] partitions noise states into two groups: impulse free states and impulse states, so that different kinds of impulsive noise can be considered in the model. The most significant advantage of this model is that bursty impulsive noise can be modelled properly because noise is allowed to stay in impulse states for a while and generate a bunch of impulses. Readers can refer to [42] for a detailed implementation.

3.4.3 A Cyclostationary Noise Model

According to the measurements conducted in indoor power network below 500 kHz in [6], noise can be assumed as cyclostationary additive Gaussian noise with zero mean and time-varying variance that is synchronous with the mains AC frequency. This is because that noise samples obtained at the same phase of different cycles follow the same Gaussian distribution with the same variance. However, when noise samples are taken at random phases, they follow the pdf of Middleton's class A model. The time-varying noise pdf is expressed by

$$p_\eta(\upsilon(iT_s)) = \frac{1}{\sqrt{2\pi\sigma^2(iT_s)}} \exp\left(-\frac{\upsilon^2(iT_s)}{2\sigma^2(iT_s)}\right) \tag{3.55}$$

where T_s is the sample period and $\sigma^2(t)$ is the periodically time-varying noise variance, as given by

$$\sigma^2(t) = \sum_{l=0}^{L-1} A_l \left|\sin\left(\frac{2\pi t}{T_0} + \theta_l\right)\right|^{n_l} \tag{3.56}$$

where T_0 is the period of AC and a set of $3L$ parameters A_l, θ_l and n_l determines the characteristic of noise. It was found that $L = 3$ is enough for approximation. In this case, the first term is a constant that represents background noise component, the

Table 3.2: Noise parameters that are required to reproduced the measurement results given in [6].

l	A_l	$\theta_l[deg]$	n_l
0	0.23	-	0
1	1.38	-6	1.91
2	7.17	-35	1.57e5

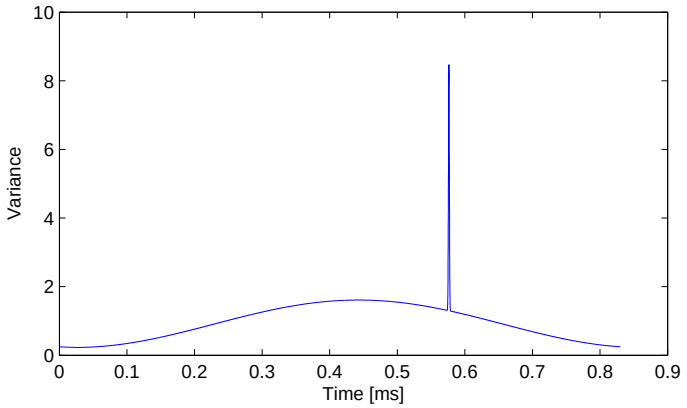

Fig. 3.14: One cycle of the cyclostationary noise variance.

second term is the periodically time-varying noise component and the third term is the periodic impulsive noise component.

Incorporating the noise PSD, three steps are required to generate the noise. First, a set of parameters are determined for the time-varying noise variance. Second, Gaussian noise with time-varying variance is generated. Finally, the noise is passed to a filter with frequency response $\sqrt{S(f)}$.

3.4.4 Simulation Results

The measurement results presented in [6] can be reproduced using the three-term time-varying variance model. The parameters are summarised in Table 3.2. The resultant noise variance is illustrated in Fig. 3.14. The mains frequency is 60 Hz. The periodic impulsive noise can be seen clearly from the variance.

Following the given steps of noise generation, and applying the noise PSD given in (3.50), the noise samples are generated and illustrated in Fig. 3.15. The amplitude of noise samples follow the shape of variance variation and some high power samples can be observed. The locations of those high power samples are consistent with the location of the periodic impulsive noise in Fig. 3.14.

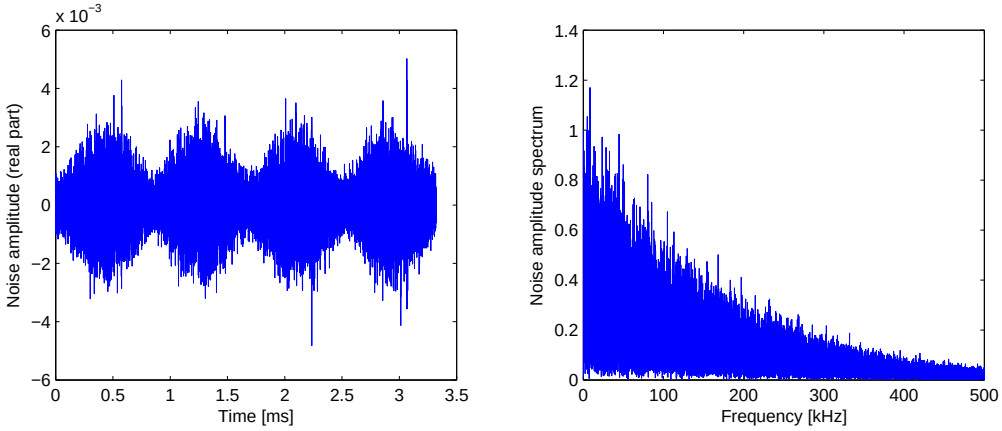

Fig. 3.15: Noise samples and its amplitude spectrum generated with the cyclostationary model.

3.5 Summary

In this chapter we first reviewed the top-down approach and bottom-up approach of power line channel modelling. We pointed out that a universally accepted power line channel model is not available especially that an accurate and reliable top-down approach is not available. On the contrary, there are accurate bottom-up approaches in literature. Then we explained the 2TL theory and the MTL theory, which are the fundamentals of bottom-up approaches. In the third part of this chapter we demonstrated an LPTV channel model which combines the voltage ratio approach proposed in [12] and the time-varying load models proposed in [5]. Based on this model, a flexible simulation tool was developed. Some key issues relating to the implementation of this tool was explained. This simulation tool is used extensively in this thesis. We also presented some sample results generated by this tool. Simulation results show that in the intervals where channel magnitude rises or falls quickly, transmitted OFDM signals may suffer from low SIR. As a conclusion, transmission in these intervals may have poor performance if channel time-variation is not properly compensated. At last, We introduced the complex noise scenario in power line channel and reviewed some representative noise models.

Chapter 4

OFDM Equalisation Over Time-Varying Power Line Channels

Latest NB-PLC standards such as ITU-T G.hnem and IEEE 1901.2 adopt OFDM. It is thus important to investigate the performance of OFDM based receivers over time-varying power line channels. OFDM equalisers with ICI mitigation capability can be categorised into linear equalisers and non-linear equalisers. Linear equalisers can be further divided into serial equalisers and block equalisers depending on whether data symbols are equalised separately or jointly. Non-linear equalisers include decision-feedback equalisers, ML equalisers, Turbo equalisers, and so on. In this chapter, three kinds of linear equalisers namely the one-tap equaliser, linear block equalisers and banded block equalisers are investigated and compared based on SINR and BER performances over a time-varying power line channel. The complexity of these equalisers are also compared.

4.1 System Model

A complex baseband-equivalent CP-OFDM system shown in Fig. 4.1 is considered in this thesis. A block of L transmit symbols $\mathbf{s} = [s_0, \ldots, s_{L-1}]^T$, corresponding to L subcarriers, is passed through an inverse fast Fourier transform (IFFT) block to obtain the time-domain signal. A cyclic prefix of length L_{cp}, which is identical to the last L_{cp} samples of the time-domain signal, is then inserted at the beginning of the signal. The transmit time-domain signal, of size $N = L + L_{cp}$, can be expressed as

$$\mathbf{t} = \mathbf{T}_{cp}\mathbf{F}^H\mathbf{s} \tag{4.1}$$

where $\mathbf{T}_{cp} = [\mathbf{I}^T_{L(cp)}\ \mathbf{I}_L]^T$ is an $N \times L$ matrix that inserts CP and $\mathbf{I}^T_{L(cp)}$ contains the last L_{cp} rows of the identity matrix $\mathbf{I}_L$, $\mathbf{F}$ is the $L \times L$ unitary discrete Fourier transform (DFT) matrix with elements $[\mathbf{F}]_{n,m} = \frac{1}{\sqrt{L}} \exp(-j2\pi nm/L)$.

After parallel-to-serial conversion, the time-domain signal sequence t_n is transmitted through a linear time-variant (LTV) power line channel with discrete impulse response

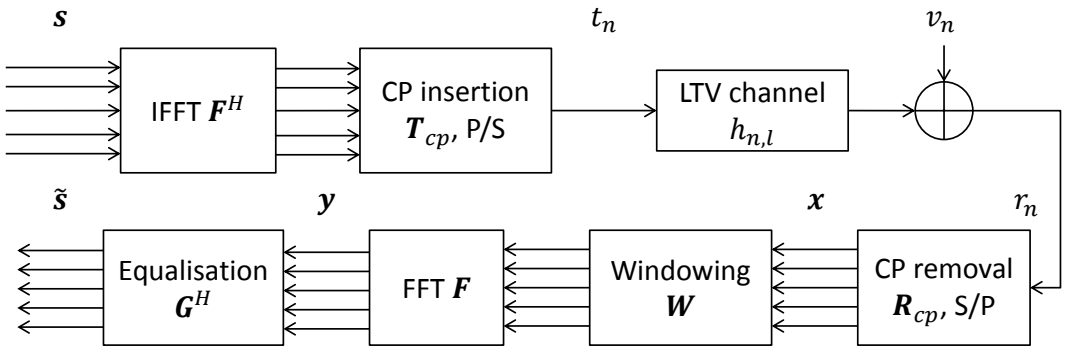

Fig. 4.1: Windowed CP-OFDM system model

$h_{n,l}$ at time n caused by an impulse applied at time $n-l$ to the channel. A finite impulse response channel with memory $L_h (L_h \leq L)$ is assumed in this thesis. Assuming perfect time and frequency synchronisation, the received signal samples can be expressed as

$$r_n = \sum_{l=0}^{L_h-1} h_{n,l} t_{n-l} + v_n \tag{4.2}$$

where v_n is noise. Although noise in PLC is complex and non-additive white Gaussian noise (AWGN), AWGN with zero mean and variance σ^2 is assumed in this thesis for simplicity. In matrix form, this can be written as

$$\mathbf{r} = \mathbf{H}\mathbf{t} + \mathbf{v} = \mathbf{H}\mathbf{T}_{cp}\mathbf{F}^H\mathbf{s} + \mathbf{v} \tag{4.3}$$

where $\mathbf{r} = [r_0, \ldots, r_{N-1}]^T$, $\mathbf{v} = [v_0, \ldots, v_{N-1}]^T$ and $\mathbf{H}$ is the $N \times N$ convolution matrix of channel with elements $[\mathbf{H}]_{n,l} = h_{n,n-l}$. Since channel memory is L_h, $[\mathbf{H}]_{n,l} = 0$ when $n - l \notin [0, L_h - 1]$.

The process of removing CP can be written in matrix form as $\mathbf{R}_{cp} = [\mathbf{0}_{L \times L_{cp}} \ \mathbf{I}_L]$. Assuming $L_{cp} \geq L_h - 1$ so that ISI is completely removed, the signal after removing CP is written as

$$\mathbf{x} = \mathbf{R}_{cp}\mathbf{H}\mathbf{T}_{cp}\mathbf{F}^H\mathbf{s} + \mathbf{R}_{cp}\mathbf{v} = \mathbf{H}_L\mathbf{F}^H\mathbf{s} + \mathbf{v}_L \tag{4.4}$$

where $\mathbf{H}_L = \mathbf{R}_{cp}\mathbf{H}\mathbf{T}_{cp}$ is an $L \times L$ circular convolution matrix with $[\mathbf{H}_L]_{n,l} = h_{n+L_{cp},\langle n-l \rangle_L}$ and $\mathbf{v}_L = \mathbf{R}_{cp}\mathbf{v}$ contains the last L samples of $\mathbf{v}$. The frequency-domain received signal is obtained by applying DFT to $\mathbf{x}$, as expressed by

$$\mathbf{y} = \mathbf{F}\mathbf{x} = \mathbf{F}\mathbf{H}_L\mathbf{F}^H\mathbf{s} + \mathbf{F}\mathbf{v}_L = \mathbf{H}_F\mathbf{s} + \mathbf{z} \tag{4.5}$$

where $\mathbf{H}_F$ is the frequency-Doppler domain channel matrix and $\mathbf{z}$ contains frequency-domain noise samples with covariance matrix $\mathbf{R}_{\mathbf{zz}} = \sigma^2\mathbf{I}_L$ since $\mathbf{F}$ is unitary.

The soft estimates $\tilde{\mathbf{s}}$ of the received symbols are obtained by applying a linear equaliser $\mathbf{G}^H$ to $\mathbf{y}$ as

$$\tilde{\mathbf{s}} = \mathbf{G}^H\mathbf{y} = \mathbf{G}^H\mathbf{H}_F\mathbf{s} + \mathbf{G}^H\mathbf{z} \tag{4.6}$$

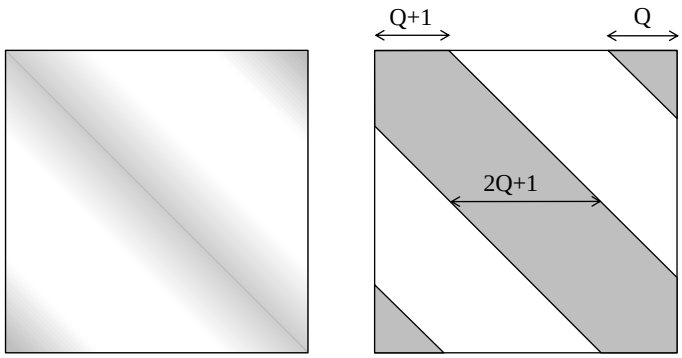

Fig. 4.2: The frequency domain channel matrix of a LTV channel

Finally, data symbols are decided from $\tilde{\mathbf{s}}$ via a symbol-by-symbol detector.

4.2 ICI Analysis

This section presents an analysis on ICI for the purposes of SINR calculation and equaliser design. In order to compare the performance improvement of using different equalisers, equaliser input SINR is also formulated.

The elements of the frequency-Doppler domain channel matrix $\mathbf{H}_F$ can be expressed as

$$[\mathbf{H}_F]_{m+d,m} = \frac{1}{L}\sum_{n=0}^{L-1}\sum_{l=0}^{L_h-1} h_{n+L_{cp},l}\exp\left(-j2\pi(ml+dn)/L\right) \tag{4.7}$$

where m represents the subcarrier index and d is the discrete Doppler index. It is easy to see that the diagonal elements (i.e. $d = 0$) of $\mathbf{H}_F$ produce the *useful signal*, while the off-diagonal elements of the mth column represents the discrete Doppler spread associated with the mth subcarrier and these elements are responsible for the ICI induced by the mth symbol on the other symbols.

Therefore, $\mathbf{H}_F$ can be split into two parts, as expressed by $\mathbf{H}_F = \mathbf{\Theta} + \mathbf{\Phi}$, where $\mathbf{\Theta}$ is the diagonal part of $\mathbf{H}_F$ and $\mathbf{\Phi} = \mathbf{H}_F - \mathbf{\Theta}$ is the corresponding off-diagonal matrix. In addition, it is proved in [13] that ICI decays rapidly as d increases. As a result, matrix $\mathbf{H}_F$ has the structure shown in Fig. 4.2(a). In this figure, the saturation of shade indicates the strength of the *useful signal* or ICI[1]. It can be seen that most of the energy is concentrated around the diagonal and two corners and, normally, the diagonal part has the highest energy.

To calculate the power of ICI, (4.5) is rewritten as

$$\mathbf{y} = \mathbf{\Theta}\mathbf{s} + \mathbf{\Phi}\mathbf{s} + \mathbf{z} \tag{4.8}$$

[1]ICI is frequency dependent, hence in practice the decay of ICI in $\mathbf{H}_F$ is irregular. Fig. 4.2(a) was drawn for illustration purpose.

where the three terms at the right hand side represent the *useful signal*, the ICI and the noise respectively. Throughout this thesis, the calculation of ICI power or SINR is based on the following assumptions.

1. data symbols and noise have zero mean
2. data symbols on different subcarriers are uncorrelated and have equal energy E_s
3. noise is independent of data symbols and the channel
4. the channel is deterministic

In addition, since ICI is frequency dependent, it is not realistic to calculate its power or SINR for each subcarrier. Instead, overall ICI power or SINR is formulated. Hence, the ICI power is written as

$$\mathcal{E}_i = \mathrm{E}[\|\mathbf{\Phi s}\|_F^2] = E_s\|\mathbf{\Phi}\|_F^2 \tag{4.9}$$

Then, the equaliser input SINR can be obtained by

$$\rho_{in} = \frac{\mathcal{E}_s}{\mathcal{E}_t - \mathcal{E}_s} = \frac{\|\mathbf{\Theta}\|_F^2}{\|\mathbf{\Phi}\|_F^2 + L\sigma^2/E_s} \tag{4.10}$$

where $\mathcal{E}_s = \mathrm{E}[\|\mathbf{\Theta s}\|_F^2]$ denotes *useful signal* power and $\mathcal{E}_t = \mathrm{E}[\|\mathbf{y}\|_F^2]$ is the total received signal power. $\mathcal{E}_t - \mathcal{E}_s$ can also be written as $\mathcal{E}_i + \mathcal{E}_n$, where $\mathcal{E}_n = L\sigma^2$ is the total noise power, since noise and ICI are independent. Specifically, when noise power is zero, SINR is maximised as $\rho_{in} = \|\mathbf{\Theta}\|_F^2/\|\mathbf{\Phi}\|_F^2$. When $\mathcal{E}_n \gg \mathcal{E}_i$, SINR can be approximated by signal-to-noise ratio (SNR). In addition to input SINR, input SIR can be obtained by removing the noise term in (4.10).

4.3 Equalisation Techniques

4.3.1 The One-tap Equaliser

The one-tap equaliser was designed for conventional OFDM systems over LTI channels. It assumes that the channel does not vary with time, hence Eq.(4.7) can be simplified to

$$\begin{aligned}[\mathbf{H}_F]_{m+d,m} &= \frac{1}{L}\sum_{n=0}^{L-1}\exp(-j2\pi dn/L)\sum_{l=0}^{L_h-1} h_l \exp(-j2\pi ml/L) \\ &= \begin{cases} \sum_{l=0}^{L_h-1} h_l \exp(-j2\pi ml/L) & d = 0 \\ 0 & d \neq 0 \end{cases}\end{aligned} \tag{4.11}$$

This indicates that $\mathbf{H}_F$ is a diagonal matrix whose diagonal is the DFT of the time-invariant channel impulse response. Thus, in the case of an LTI channel, It is straightforward to choose the equaliser coefficients as $\mathbf{G}^H = \mathbf{H}_F^{-1}$. Since $\mathbf{H}_F$ is a diagonal matrix, its inverse can be obtained easily.

In the case of an LTV channel, the one-tap equaliser uses only the diagonal of $\mathbf{H}_F$. Hence it can be written as

$$\mathbf{G}_{ot}^H = \mathcal{D}(\mathbf{H}_F)^{-1} = \mathbf{\Theta}^{-1} \tag{4.12}$$

In fact, the diagonal of $\mathbf{H}_F$ is the DFT of time-averaged channel impulse response hence knowledge of the full channel matrix $\mathbf{H}_F$ is not necessary. Nevertheless, it should be noted that the one-tap equaliser ignores the effect of ICI so that severe performance degradation should be expected.

4.3.2 Linear Block Equalisers

Linear block equalisers perform equalisation on all the subcarriers of an OFDM block jointly. This usually requires a full equalisation matrix $\mathbf{G}^H$ with $L \times L$ coefficients. Usually, $\mathbf{G}^H$ is determined based on the least square (LS) method or the MMSE method. The solutions[2] to these two methods show that the equalisation matrix can be expressed as

$$\mathbf{G}_{zf}^H = \mathbf{H}_F^\dagger = \mathbf{H}_F^H(\mathbf{H}_F\mathbf{H}_F^H)^{-1} \tag{4.13}$$

$$\mathbf{G}_{mmse}^H = \mathbf{H}_F^H(\mathbf{H}_F\mathbf{H}_F^H + \sigma^2\mathbf{I}_L)^{-1} \tag{4.14}$$

where $\mathbf{H}_F^\dagger = \mathbf{H}_F^H(\mathbf{H}_F\mathbf{H}_F^H)^{-1}$ is the pseudo-inverse of $\mathbf{H}_F$. Since $\mathbf{G}_{zf}^H$ zeros out interference elements in $\mathbf{H}_F$, it is also called zero forcing (ZF) equalisation in communications. Although ZF equalisation removes interference completely, noise is not considered and sometimes noise power may be enhanced. MMSE equalisation is a more general method in that it considers the effect of noise. It provides a better balance between interference and noise, despite the presentation of residual interference. When noise power is zero (i.e. $\sigma^2 = 0$), MMSE is reduced to ZF.

4.3.3 Banded Block Equalisers

According to the structure of $\mathbf{H}_F$ shown in Fig. 4.2(a), ICI from faraway subcarriers has negligible power. Therefore, the channel matrix $\mathbf{H}_F$ can be approximated by a banded matrix $\mathbf{B}_F$ by ignoring those negligible ICI elements. Fig. 4.2(b) shows the structure of a banded matrix, in which the elements inside the band (the shades) are retained while other out-of-band (OOB) elements are all set to zero. Q denotes the number of retained superdiagonals and subdiagonals (Q superdiagonals and Q subdiagonals). This approximation can be expressed as

$$\mathbf{B}_F = \mathbf{H}_F \circ \mathbf{T}^{(Q)} \tag{4.15}$$

[2]Due to the popularity of these two methods, their derivations are not presented here.

where $\mathbf{T}^{(Q)}$ is an $L \times L$ Toeplitz matrix whose first row $\mathbf{t}_1^{(Q)}$ is

$$\mathbf{t}_1^{(Q)} = [\overbrace{1, \ldots, 1}^{Q+1 \text{ ones}}, 0, \ldots, 0, \overbrace{1, \ldots, 1}^{Q \text{ ones}}] \tag{4.16}$$

Banded versions of ZF and MMSE are obtained by replacing the $\mathbf{H}_F$ in (4.13) and (4.14) with $\mathbf{B}_F$, as expressed by

$$\mathbf{G}_{zf|B}^H = \mathbf{B}_F^\dagger = \mathbf{B}_F^H(\mathbf{B}_F\mathbf{B}_F^H)^{-1} \tag{4.17}$$

$$\mathbf{G}_{mmse|B}^H = \mathbf{B}_F^H(\mathbf{B}_F\mathbf{B}_F^H + \sigma^2\mathbf{I}_L)^{-1} \tag{4.18}$$

Similarly, $\mathbf{B}_F^\dagger$ is the pseudo-inverse of $\mathbf{B}_F$.

The purpose of using banded channel matrices is to reduce computational complexity. Obviously, number of multiplications is reduced due to the zeros in $\mathbf{B}_F$. The complexity of matrix inversions involved in (4.17) and (4.18) can be reduced by adopting low-complexity matrix decompositions such as Cholesky or LDL^H factorisation [46].

4.4 Performance and Complexity Analysis

The ICI mitigation ability of different equalisers are analysed based on their output SINRs. The SINR can be formulated when the frequency-Doppler domain channel matrix $\mathbf{H}_F$ is available. Due to the difficulties in formulating BER, BER performances will be compared through Monte Carlo simulation in the next section.

The formulation is performed on the equalised signal samples $\tilde{\mathbf{s}}$ in (4.6). Similar to (4.10), the generalised output SINR can be written as

$$\rho_{out} = \frac{\mathcal{E}_s}{\mathcal{E}_t - \mathcal{E}_s} = \frac{\|\mathcal{D}(\mathbf{G}^H\mathbf{H}_F)\|_F^2}{\|\mathbf{G}^H\mathbf{H}_F - \mathcal{D}(\mathbf{G}^H\mathbf{H}_F)\|_F^2 + \sigma^2\|\mathbf{G}^H\|_F^2} \tag{4.19}$$

where it is assumed that symbol energy E_s is unity. From (4.19), the output SINR of the aforementioned three equalisers are formulated as

$$\rho_{ot} = \frac{L}{\|\mathbf{G}_{ot}^H\mathbf{H}_F\|_F^2 + \sigma^2\|\mathbf{G}_{ot}^H\|_F^2 - L} \tag{4.20}$$

$$\rho_{zf} = \frac{L}{\sigma^2\|\mathbf{G}_{zf}^H\|_F^2} \tag{4.21}$$

$$\rho_{mmse} = \frac{\|\mathcal{D}(\mathbf{G}_{mmse}^H\mathbf{H}_F)\|_F^2}{\|\mathbf{G}_{mmse}^H\mathbf{H}_F\|_F^2 + \sigma^2\|\mathbf{G}_{mmse}^H\|_F^2 - \|\mathcal{D}(\mathbf{G}_{mmse}^H\mathbf{H}_F)\|_F^2} \tag{4.22}$$

Generally speaking for all the three equalisers, SINR is close to SNR at low SNR region since noise dominates interference. For the one-tap equaliser, since it has no ICI mitigation capability, the performance will be limited by ICI. Hence, the corresponding SINR should be upper bounded by the input SIR. For ZF equalisers, there is always a gap between SNR and its SINR and this gap can be quantified by $\|\mathbf{G}_{zf}^H\|_F^2/L$. Since MMSE can be reduced to ZF when noise is absent, its performance can be expected

to be close to ZF when noise power is low. Nevertheless, it should be expected that MMSE outperforms ZF when noise power is high.

The output SINRs of the banded ZF and MMSE equalisers are formulated by substituting the corresponding equaliser matrices into (4.19). In general, since banded equalisers mitigate part of the ICI, some performance degradation should be expected, especially at high SNR region when ICI is dominate. Furthermore, the performance depends on the choice of Q since it determines the amount of ICI that is ignored. This neglected OOB interference power is defined by $\|\mathbf{H}_F - \mathbf{B}_F\|_F^2$.

Among these equalisers, the one-tap equaliser has the lowest complexity, which involves only L inversions for the equaliser matrix $\mathbf{G}_{ot}^H$. Both full block ZF and MMSE have very high complexity that can be represented by $\mathcal{O}(L^3)$. The banded ZF and MMSE equalisers using LDL^H factorisation for matrix inversions have a complexity of $\mathcal{O}(Q^2L)$ [46].

Clearly, for banded equaliser, the choice of Q is a tradeoff between performance and complexity. It is usually chosen according to some empirical rules in wireless communication. For example, it can be chosen in proportion to f_d, which is the maximum Doppler frequency normalised to subcarrier spacing, or as the value that reduces the OOB interference power below certain threshold. It was found in [13] that $Q = \lceil f_d \rceil + 1$ provides a good balance between performance and complexity. In practice, Q usually takes single-digit values and this is true for PLC as well. Therefore, banded equalisers have a much lower complexity than full block equalisers.

4.5 Simulation Results

This section first presents some numerical results about the equaliser output SINR when the aforementioned equalisers are applied to a CP-OFDM system over the sample power line channel shown in Fig. 3.11. In order to show the SINR improvement of different equalisers, the equaliser input SINR will also be presented as a reference. At last, BER performances that are obtained through Monte Carlo simulation will be given.

The CP-OFDM system assumed in simulation is modified from the system proposed in the PRIME standard. The same subcarrier spacing, which is 488.28125 Hz, is used while the number of subcarriers is extended to 512 in order to make sure the signal covers most of the NB-PLC frequency band. No guard bands or virtual subcarriers is applied and a CP length of 48 samples is adopted. As a result, the signal covers the frequency band between 0 and 250 kHz and the total length of an OFDM block is 2240 us. ICI could be severe to such a system due to the narrow subcarrier spacing (or a long OFDM block). Without loss of generality, quadrature phase shift keying (QPSK) is assumed in this thesis.

Since power line channels are deterministic, a single channel realisation shown in Fig. 3.11 is considered in this simulation. For a 50 Hz AC power system, 8 complete

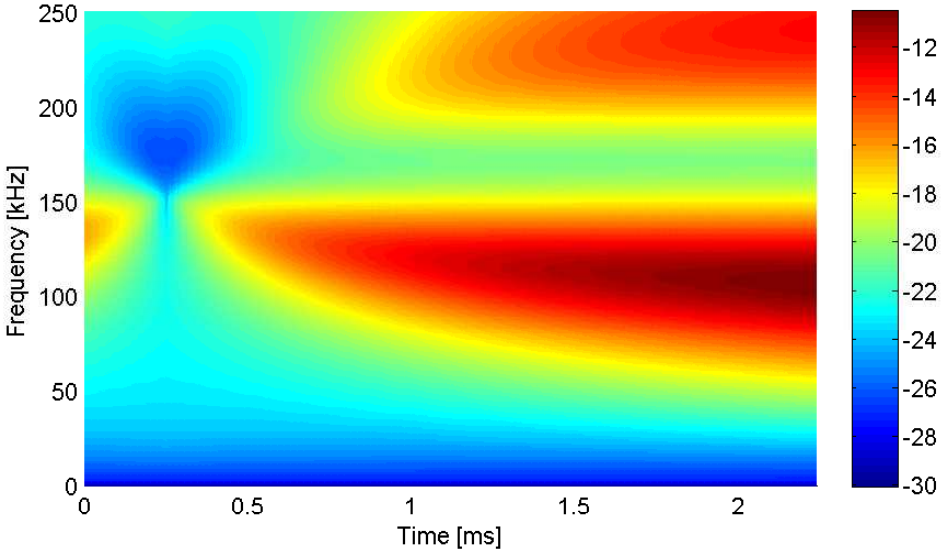

Fig. 4.3: The 4^{th} section of the power line channel shown in Fig. 3.11

OFDM blocks can be transmitted within a period. Accordingly, the channel is divided into 8 sections in time and the corresponding input SIR is calculated for each section. Then the section with the lowest input SIR is used for performance comparison. For this particular channel realisation, the 4^{th} section (shown in Fig. 4.3) has the lowest input SIR which is about 10 dB.

The comparison of SINR performance under different conditions is illustrated in Fig. 4.4. In this figure, the SNR curve and input SIR curve are plotted as references. It can be seen that the input SINR is limited by SNR (i.e. noise power) at low SNR region and input SIR (i.e. interference power) at high SNR region. This is true for the one-tap equaliser as well but its SINR performance is worse. This indicates that the one-tap equaliser does not help improving SINR. Instead, it enhances noise and interference power.

The ZF and MMSE equalisers perform very well in improving output SINR at high SNR region. This means that both ZF and MMSE have very good interference mitigation capabilities. However, at low SNR region, their performances are still limited by noise. For MMSE, this can be seen from the fact that its performance is limited by the input SINR. For ZF, its output SINR at low SNR region indicates that it enhances noise power. The performances of banded ZF and MMSE equalisers at low SNR region are very close to those of ordinary ZF and MMSE equalisers because they have the same ability to reduce the effect of noise. However, at high SNR region, their performances are limited by residual interference which depends on the choice of Q. Clearly, as Q increases, their performances will eventually equal to those of ordinary ZF and MMSE equalisers. In fact, the one-tap equaliser is a special case of banded ZF equalisers when $Q = 0$. Therefore, the performances of banded ZF and MMSE equalisers can

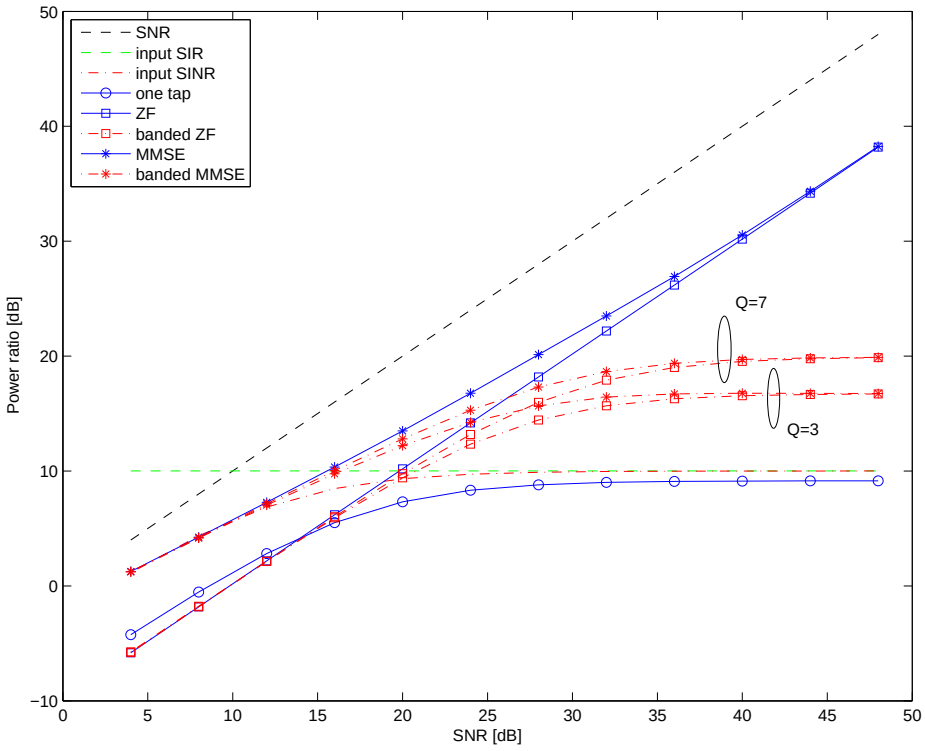

Fig. 4.4: SINR performance under different conditions

be expected to be between one-tap equalisers and ordinary ZF and MMSE equalisers depending on the value of Q.

BER performances are shown in Fig. 4.5. As expected, the one-tap equaliser suffers from a quite high error floor while the MMSE equaliser shows the best performance. The ZF equaliser performs slightly worse than the MMSE equaliser. The banded equalisers suffer from error floors as well. Again, this is because of the OOB interference controlled by the bandwidth Q.

4.6 Summary

Among the discussed linear block equalisers, the one-tap equaliser and the MMSE equaliser are two extreme cases. The MMSE equaliser performs the best but has a very high complexity while the one-tap equaliser is very simple but has no ICI mitigation capability. The ZF equaliser performs worse than the MMSE equaliser but it has the same complexity as the latter. The only advantage of ZF over MMSE is that it does not require the knowledge of noise power. The performance and complexity of banded equalisers are between those of the one-tap equaliser and the ordinary ZF and MMSE equalisers. The advantage of banded equalisers is that the performance-

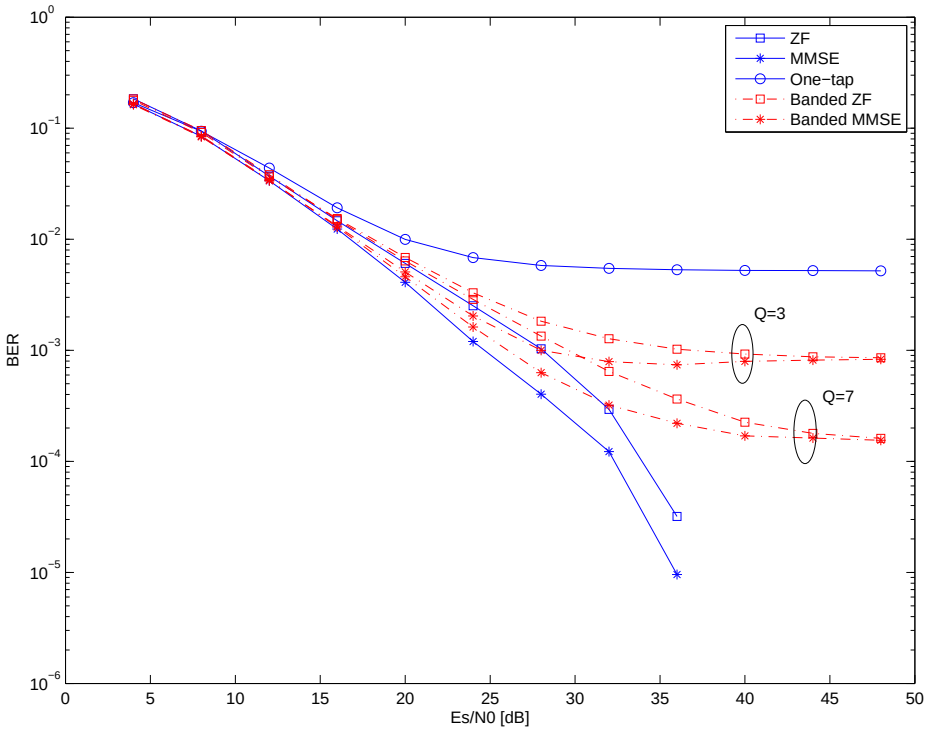

Fig. 4.5: BER performance under different conditions

complexity tradeoff can be controlled according to needs. Apparently, to improve the performance of banded equalisers, Q has to be increased, but this will in turn increase the complexity. In order to achieve a good BER performance, Q may have to be large hence a high complexity. In order to achieve a better performance-complexity tradeoff, receiver windowing is sometimes cooperated with banded equalisers. The design of optimal receiver windows is discussed in the next chapter.

Chapter 5

Receiver Windowing

This chapter investigates the possibility of using time-domain receiver windows to help improving the performance-complexity tradeoff of banded equalisers. Time-domain receiver windows have the ability to shape the spectrum of the received signal so that signal power that is leaked to adjacent subcarriers maybe reduced. It should be noted that receiver windowing does not affect the performance of non-banded linear block equalisers since its effect is completely removed during equalisation. However, when it is cooperated with band approximation, the OOB interference power can be greatly reduced, thereby improving performance considerably.

Some window design criteria for wireless communication over time-varying frequency selective channel can be found in the literature. Although the methods are different, they all aim at reducing OOB interference. In this chapter, we investigate three window design criteria. The first one is proposed in [14] and it aims at minimising the band approximation error (BAE). Since this criterion is designed for wireless communication, a simplification that is not valid over time-varying power line channels is applied, which hence causes a bad performance when this is used for PLC. Our research have shown that by cancelling the simplification, this criterion works well for PLC. The other two criteria attempt to maximise the modified input SINR. The one proposed in [13] defines the input SINR as the in-band signal power over the OOB interference power plus noise power. However, it has been found that this criterion works poorly over time-varying power line channels. Therefore, we propose a modified approach with a different definition of input SINR. Simulations have shown that our proposal outperforms the other two criteria.

Our contributions can be summarised into three points. First, this is the first time that receiver windowing is investigated over time-varying power line channels. Second, we have found that some good window design criteria that were developed for wireless communication do not work properly over time-varying power line channels. Finally, we propose a modified maximum input SINR criterion which has been proved a better approach for PLC than the other two criteria.

5.1 System Model

Time-domain receiver window is applied before the fast Fourier transform (FFT) operation. Window coefficients are denoted by the vector $\mathbf{w} = [w_0, \ldots, w_{L-1}]^T$. The signal after removing CP is left-multiplied by the window matrix $\mathbf{W} = \mathcal{D}(\mathbf{w})$ and then the DFT matrix $\mathbf{F}$. From (4.4), this is written as

$$\mathbf{y}^{(w)} = \mathbf{FWx} = \mathbf{FWH}_L\mathbf{F}^H\mathbf{s} + \mathbf{FWv}_L = \mathbf{H}_F^{(w)}\mathbf{s} + \mathbf{z}^{(w)} \tag{5.1}$$

where $\mathbf{H}_F^{(w)}$ is the windowed frequency-Doppler domain channel matrix and it can be decomposed into

$$\mathbf{H}_F^{(w)} = \mathbf{FWF}^H\mathbf{FH}_L\mathbf{F}^H = \mathbf{W}_F\mathbf{H}_F \tag{5.2}$$

in which $\mathbf{W}_F$ is a circulant window matrix in the frequency-Doppler domain. $\mathbf{z}^{(w)} = \mathbf{W}_F\mathbf{Fv}_L$ is the frequency-domain filtered noise vector with covariance matrix $\mathbf{R}_{\mathbf{zz}}^{(w)} = \sigma^2\mathbf{W}_F\mathbf{W}_F^H$. It is interesting to note that the noise is Gaussian but no longer white.

In this case, band approximation is denoted by $\mathbf{B}_F^{(w)} = \mathbf{H}_F^{(w)} \circ \mathbf{T}^{(Q)}$. Then, the soft estimates are expressed by

$$\tilde{\mathbf{s}}^{(w)} = \mathbf{G}^{(w)H}\mathbf{y}^{(w)} = \mathbf{G}^{(w)H}\mathbf{H}_F^{(w)}\mathbf{s} + \mathbf{G}^{(w)H}\mathbf{z}^{(w)} \tag{5.3}$$

where $\mathbf{G}^{(w)H}$ denotes the equaliser coefficients for windowed OFDM. Take MMSE as an example, $\mathbf{G}^{(w)H}$ is expressed as

$$\mathbf{G}_{mmse}^{(w)H} = \mathbf{B}_F^{(w)H}(\mathbf{B}_F^{(w)}\mathbf{B}_F^{(w)H} + \sigma^2\mathbf{W}_F\mathbf{W}_F^H)^{-1} \tag{5.4}$$

where we use the noise covariance matrix $\mathbf{R}_{\mathbf{zz}}^{(w)}$ to cope with the coloured noise.

5.2 Window Design Criteria

From a performance point of view, a good window design criterion could be the optimisation of SINR or mean squared error (MSE) on the decision variable. However, a closed-form solution to such kind of optimisation problem is difficult to find [21]. Therefore, it is common to formulate the optimisation problem on the received signal before equalisation.

In this section, we introduce three window design criteria. The first one minimises the BAE [14]. The second one attempts to maximise the modified input SINR [13], which is defined as the in-band signal to out-of-band interference noise ratio (IONR). In order to distinguish it from the ordinary input SINR, we use the abbreviation IONR. Finally, we propose a new window design criterion that is based on a new definition of input SINR, which is the *useful signal* to out-of-band interference noise ratio (SONR).

5.2.1 The Minimum BAE Criterion

We first introduce the minimum BAE criterion. The BAE is defined as $\mathbf{E}^{(w)} = \mathbf{H}_F^{(w)} - \mathbf{B}_F^{(w)}$. The criterion aims at minimising the mean squared BAE, as expressed by

$$\mathbf{w}_\star = \arg\min_{\mathbf{w}} \mathrm{E}[\|\mathbf{E}^{(w)}\|_F^2] \tag{5.5}$$

subject to the energy constraint $\mathbf{w}^H\mathbf{w} = L$. As explained in appendix A, when the channel has a constant energy over time, the term $\mathrm{E}[\|\mathbf{H}_F^{(w)}\|_F^2]$ in the mean squared BAE is a constant. This indicates that the problem can be simplified to maximising $\mathrm{E}[\|\mathbf{B}_F^{(w)}\|_F^2]$, which, in full expression, is

$$\mathbf{w}_\star = \arg\max_{\mathbf{w}} \mathrm{E}[\|\mathbf{B}_F^{(w)}\|_F^2] \tag{5.6}$$

This simplification was first proposed in [14]. However, for a power line channel with a time-varying channel energy, this simplification is not valid and (5.5) has to be used. Therefore, in this chapter, we discuss both cases with a focus on power line channels.

After some derivations (see appendix A), the optimisation functions, for the two kinds of channels, are written as

$$\mathbf{w}_\star = \arg\min_{\mathbf{w}} \mathrm{E}[\|\mathbf{E}^{(w)}\|_F^2] = \arg\min_{\mathbf{w}} \{\mathbf{w}^H(\mathbf{R}_{\mathcal{H}\mathcal{H}} \circ (\mathbf{I}_L - \mathbf{A}))\mathbf{w}\} \tag{5.7}$$

$$\mathbf{w}_\star = \arg\max_{\mathbf{w}} \mathrm{E}[\|\mathbf{B}_F^{(w)}\|_F^2] = \arg\max_{\mathbf{w}} \{\mathbf{w}^H(\mathbf{R}_{\mathcal{H}\mathcal{H}} \circ \mathbf{A})\mathbf{w}\} \tag{5.8}$$

where $[\mathcal{H}]_{n,l} = h_{n,l}$ is obtained from $\mathbf{H}_L$ by rearranging the diagonals as columns, $\mathbf{R}_{\mathcal{H}\mathcal{H}} = \mathrm{E}[\mathcal{H}\mathcal{H}^H]$ is the time autocorrelation matrix of channel, and $\mathbf{A}$ is defined as

$$[\mathbf{A}]_{m,n} = \begin{cases} (2Q+1)/L & m = n \\ \dfrac{\sin(\pi(2Q+1)(n-m)/L}{L\sin(\pi(n-m)/L)} & m \neq n \end{cases} \tag{5.9}$$

In this thesis, (5.7) and (5.8) are used for power line channels and wireless channels respectively. The optimisation functions can be solved by doing eigenvalue decomposition to $\mathbf{R}_{\mathcal{H}\mathcal{H}} \circ (\mathbf{I}_L - \mathbf{A})$ for (5.7) or $\mathbf{R}_{\mathcal{H}\mathcal{H}} \circ \mathbf{A}$ for (5.8). The optimal solution $\mathbf{w}_\star$ is the eigenvector that corresponds to the smallest eigenvalue of $\mathbf{R}_{\mathcal{H}\mathcal{H}} \circ (\mathbf{I}_L - \mathbf{A})$ for (5.7) or the largest eigenvalue of $\mathbf{R}_{\mathcal{H}\mathcal{H}} \circ \mathbf{A}$ for (5.8).

5.2.2 The Maximum IONR Criterion

The window coefficients $\mathbf{w}$ are designed to maximise the IONR. To aid in the definition of "in-band signal" and "OOB interference", we rewrite (5.1) as

$$\mathbf{y}^{(w)} = \mathbf{B}_F^{(w)}\mathbf{s} + \mathbf{E}^{(w)}\mathbf{s} + \mathbf{z}^{(w)} \tag{5.10}$$

where $\mathbf{B}_F^{(w)}\mathbf{s}$ and $\mathbf{E}^{(w)}\mathbf{s}$ gives the "in-band signal" and "OOB interference" respectively. The in-band signal power $\mathcal{P}_{ib}$ and OOB interference power $\mathcal{P}_{oob}$ are then defined by

$$\mathcal{P}_{ib} = \mathrm{E}[\|\mathbf{B}_F^{(w)}\|_F^2] \tag{5.11}$$

$$\mathcal{P}_{oob} = \mathrm{E}[\|\mathbf{E}^{(w)}\|_F^2] = \mathrm{E}[\|\mathbf{H}_F^{(w)}\|_F^2] - \mathcal{P}_{ib} \tag{5.12}$$

Note that the OOB interference power is equivalent to the mean squared BAE. In addition, noise power can be written as $\mathcal{P}_n = \mathrm{E}[\|\mathbf{z}^{(w)}\|_F^2] = \sigma^2\mathbf{w}^H\mathbf{w} = \sigma^2 L$. The IONR is defined mathematically as

$$\mathrm{IONR}(\mathbf{w}) = \frac{\mathcal{P}_{ib}}{\mathcal{P}_{oob} + \mathcal{P}_n} = \frac{\mathcal{P}_{ib}}{\mathcal{P}_t - \mathcal{P}_{ib}} \tag{5.13}$$

where $\mathcal{P}_t = \mathrm{E}[\|\mathbf{y}^{(w)}\|_F^2]$ is the total received signal power. The window coefficients $\mathbf{w}_\star$ that maximise IONR are derived in appendix B and the result shows that they can be found by

$$\begin{aligned}\mathbf{w}_\star &= \arg\max_{\mathbf{w}} \mathrm{IONR}(\mathbf{w}) \\ &= \mathbf{v}_\star(\mathbf{R}_{\mathcal{H}\mathcal{H}} \circ \mathbf{A},\ \mathcal{D}(\mathbf{R}_{\mathcal{H}\mathcal{H}} + \sigma^2\mathbf{I}_L) - \mathbf{R}_{\mathcal{H}\mathcal{H}} \circ \mathbf{A})\end{aligned} \tag{5.14}$$

where $\mathbf{v}_\star(\mathbf{A}, \mathbf{B})$ denotes the principle generalised eigenvector [47] of the matrix pair $(\mathbf{A}, \mathbf{B})$.

5.2.3 The Maximum SONR Criterion

This criterion uses *useful signal* power instead of in-band signal power for the design of window coefficients. In this case, (5.1) is rewritten as

$$\mathbf{y}^{(w)} = \mathbf{\Omega}^{(w)}\mathbf{s} + \mathbf{\Psi}^{(w)}\mathbf{s} + \mathbf{E}^{(w)}\mathbf{s} + \mathbf{z}^{(w)} \tag{5.15}$$

where $\mathbf{\Omega}^{(w)}\mathbf{s} = \mathcal{D}(\mathbf{B}_F^{(w)})\mathbf{s}$ is the *useful signal* and $\mathbf{\Psi}^{(w)}\mathbf{s} = (\mathbf{B}_F^{(w)} - \mathbf{\Omega}^{(w)})\mathbf{s}$ denotes the in-band interference signal. Hence, the *useful signal* power is defined as $\mathcal{P}_s = \mathrm{E}[\|\mathbf{\Omega}^{(w)}\|_F^2]$. As a result, the SONR is defined as

$$\mathrm{SONR}(\mathbf{w}) = \frac{\mathcal{P}_s}{\mathcal{P}_{oob} + \mathcal{P}_n} = \frac{\mathcal{P}_s}{\mathcal{P}_t - \mathcal{P}_{ib}} \tag{5.16}$$

where it can be seen that the in-band interference power, which is defined as $\mathcal{P}_{ibi} = \mathrm{E}[\|\mathbf{\Psi}^{(w)}\|_F^2]$, is treated as *don't care*. The window coefficients $\mathbf{w}_\star$ that maximise SONR can be found by (see appendix B)

$$\begin{aligned}\mathbf{w}_\star &= \arg\max_{\mathbf{w}} \mathrm{SONR}(\mathbf{w}) \\ &= \mathbf{v}_\star(\mathbf{R}_{\mathcal{H}\mathcal{H}}/L,\ \mathcal{D}(\mathbf{R}_{\mathcal{H}\mathcal{H}} + \sigma^2\mathbf{I}_L) - \mathbf{R}_{\mathcal{H}\mathcal{H}} \circ \mathbf{A})\end{aligned} \tag{5.17}$$

This solution is slightly different from (5.14) but as will be discussed in the next two sections, it works much better over time-varying power line channels.

It should be noted that all the window design criteria depend on the channel time autocorrelation $\mathbf{R}_{\mathcal{H}\mathcal{H}}$. In wireless communication, this is usually determined by the channel Doppler spectrum. For example, if Jakes Doppler spectrum [48] is assumed, the autocorrelation matrix can be expressed by $[\mathbf{R}_{\mathcal{H}\mathcal{H}}]_{m,n} = J_0(2\pi f_d(m-n)/L)$, where $J_0(\cdot)$ denotes the zeroth-order Bessel function of the first kind. Obviously, the window is fixed when f_d is a constant over time. On the contrary, since power line channel is deterministic, $\mathbf{R}_{\mathcal{H}\mathcal{H}} = \mathcal{H}\mathcal{H}^H$ and it has to be calculated for each OFDM block if the channel is time-varying.

5.2.4 The SOE Constraint

As mentioned in chapter 4, when LDL^H factorisation is used with banded equalisation, the complexity of equalisation can be significantly reduced. However, the term $(\mathbf{B}_F^{(w)}\mathbf{B}_F^{(w)H} + \sigma^2\mathbf{W}_F\mathbf{W}_F^H)^{-1}$ in MMSE equalisation is not banded because the noise covariance matrix $\mathbf{R}_{\mathbf{zz}}^{(w)}$ is not banded. To solve this problem, Rugini [14] proposed to apply the additional sum-of-exponentials (SOE) constraint to the minimum BAE criterion, as expressed by

$$[\mathbf{w}]_l = \sum_{q=-Q}^{Q} b_q \exp\left(j2\pi ql/L\right) \tag{5.18}$$

where the coefficients $\{b_q\}$ represent the weightings of the exponentials. This constraint ensures that the noise covariance matrix $\mathbf{R}_{\mathbf{zz}}^{(w)}$ is banded with upper and lower bandwidth $2Q$ so that LDL^H factorisation can still be exploited. The SOE constraint can also be written in matrix form as

$$\mathbf{w} = \tilde{\mathbf{F}}\mathbf{b} \tag{5.19}$$

where $\mathbf{b} = [b_{-Q}, \ldots, b_Q]^T$ and $\tilde{\mathbf{F}} = [\mathbf{f}_{L-Q+1}, \ldots, \mathbf{f}_L, \mathbf{f}_0, \mathbf{f}_1, \ldots, \mathbf{f}_Q]$ contains the last Q and first $Q+1$ columns of the DFT matrix $\sqrt{L}\mathbf{F}$, and $\mathbf{f}_l$ denotes the l^{th} column of the DFT matrix $\sqrt{L}\mathbf{F}$.

In fact, this constraint can be applied to all the three window design criteria. When it is applied, the optimisation problem will be to find an optimal set of weightings $\mathbf{b}_\star$. Taking (5.8) as an example, the optimisation function becomes

$$\mathbf{b}_\star = \arg\max_{\mathbf{b}} \{\mathbf{b}^H\tilde{\mathbf{F}}^H(\mathbf{R}_{\mathcal{H}\mathcal{H}} \circ \mathbf{A})\tilde{\mathbf{F}}\mathbf{b}\} \tag{5.20}$$

The optimal $\mathbf{b}_\star$ is obtained by solving the eigenvalue problem on $\tilde{\mathbf{F}}^H(\mathbf{R}_{\mathcal{H}\mathcal{H}} \circ \mathbf{A})\tilde{\mathbf{F}}$. The optimal window is then given by substituting $\mathbf{b}_\star$ into (5.19).

5.3 Discussion and Simulation Results

In this section we first compare the performance of the BAE and IONR criteria. Then we show the advantage of the proposed maximum SONR criterion in the presence

of noise. We also discuss the effect of noise, Q and the SOE constraint in window design. Finally, we show the BER performance of the three window design criteria. The discussion presented in this section is assisted by simulation with the channel realisation given in Fig. 4.3. The simulation setup is the same as the one adopted in chapter 4. For clarity, ZF is not considered in this section.

5.3.1 Minimum BAE versus Maximum IONR

We first compare the minimum BAE criterion and the maximum IONR criterion. To do so, we rewrite the IONR in another form as

$$\mathrm{IONR}(\mathbf{w}) = \left(\frac{\mathbf{w}^H \mathcal{D}(\mathbf{R}_{\mathcal{H}\mathcal{H}} + \sigma^2 \mathbf{I}_L)\mathbf{w}}{\mathbf{w}^H (\mathbf{R}_{\mathcal{H}\mathcal{H}} \circ \mathbf{A})\mathbf{w}} - 1 \right)^{-1} \tag{5.21}$$

This indicates that maximising IONR is equivalent to minimising $\frac{\mathbf{w}^H \mathcal{D}(\mathbf{R}_{\mathcal{H}\mathcal{H}} + \sigma^2 \mathbf{I}_L)\mathbf{w}}{\mathbf{w}^H (\mathbf{R}_{\mathcal{H}\mathcal{H}} \circ \mathbf{A})\mathbf{w}}$. When the channel is wireless, using the same assumptions as are used in appendix A, the numerator is a constant as $\mathbf{w}^H \mathcal{D}(\mathbf{R}_{\mathcal{H}\mathcal{H}} + \sigma^2 \mathbf{I}_L)\mathbf{w} = (\mathcal{E}_h + \sigma^2)L$. Thus, the problem can be further simplified to maximising $\mathbf{w}^H (\mathbf{R}_{\mathcal{H}\mathcal{H}} \circ \mathbf{A})\mathbf{w}$, which is the same as (5.8). As a result, the minimum BAE criterion and the maximum IONR criterion are equivalent for wireless channels, and noise plays an irrelevant role in the maximum IONR criterion.

As for power line channels, we first assume noise power is zero and rewrite the optimisation functions of the two criteria as

$$\arg\max_{\mathbf{w}} \mathrm{IONR}(\mathbf{w}) = \arg\min_{\mathbf{w}} \frac{\mathbf{w}^H \mathcal{D}(\mathbf{R}_{\mathcal{H}\mathcal{H}})\mathbf{w}}{\mathbf{w}^H (\mathbf{R}_{\mathcal{H}\mathcal{H}} \circ \mathbf{A})\mathbf{w}} \tag{5.22}$$

$$\arg\min_{\mathbf{w}} \mathrm{E}[\|\mathbf{E}^{(w)}\|_F^2] = \arg\min_{\mathbf{w}} \{\mathbf{w}^H \mathcal{D}(\mathbf{R}_{\mathcal{H}\mathcal{H}})\mathbf{w} - \mathbf{w}^H (\mathbf{R}_{\mathcal{H}\mathcal{H}} \circ \mathbf{A})\mathbf{w}\} \tag{5.23}$$

Clearly, the maximum IONR criterion tries to minimise the ratio of $\mathbf{w}^H \mathcal{D}(\mathbf{R}_{\mathcal{H}\mathcal{H}})\mathbf{w}$ to $\mathbf{w}^H (\mathbf{R}_{\mathcal{H}\mathcal{H}} \circ \mathbf{A})\mathbf{w}$ while the minimum BAE criterion attempts to minimise the difference between them.

It is hard to compare these two methods mathematically since no closed form solutions can be found for optimising windows. In this thesis, we compare the window design criteria from three aspects. First, the amplitude spectrum of designed windows are compared intuitively. Second we compare the input SINR using (4.10). Finally, we compare the ultimate BER performance.

Simulation results have shown that when noise is not considered, these two criteria generate almost the same window. In fact, under the same assumption, the maximum SONR criterion also generates a very similar window. It is interesting to note that these three criteria have the common part, the BAE $\mathbf{w}^H (\mathcal{D}(\mathbf{R}_{\mathcal{H}\mathcal{H}}) - \mathbf{R}_{\mathcal{H}\mathcal{H}} \circ \mathbf{A})\mathbf{w}$. This may indicate that BAE dominates the optimisation. Nevertheless, when noise is considered in the IONR criterion, it generates completely different windows and its BER performance becomes very worse. The effect of noise is discussed in the next subsection in details.

5.3.2 The Advantage of the Maximum SONR Criterion in the Presence of Noise

To show the effect of noise, we plot the input SINR with respect to SNR in Fig. 5.1. The windows are generated with the channel in Fig. 4.3 when $Q = 3$. First of all, the input SINRs induced by these three windows are significantly lower than that shown in Fig. 4.4. This is because to reduce OOB interference, it is generally unavoidably that in-band interference may be increased while *useful signal* may be reduced[1]. Specifically, the SONR window shows the highest input SINR while the IONR window shows the lowest input SINR. It is interesting to note that the input SINR induced by the SONR window decreases at high SNR region.

To understand the cause of these behaviours, we plot the amplitude spectrum of the three windows in the cases of very low and very high SNR. When SNR is high, it can be observed that the SONR window and the IONR window are close to the BAE window. This is consistent with the finding presented in the previous subsection that these three criteria generate similar results when there is no noise. When noise power is high, it boosts up the total signal power. For the IONR window, in order to deal with the additional signal power introduced by noise, in-band signal power is increased as a whole, which in turn increases in-band interference power and reduces input SINR. For the SONR window, *useful signal* power is enhanced or at least maintained at a high level (higher than the BAE window) while in-band interference power is controlled at a relatively low level. Therefore, the SONR window shows a better input SINR. The maximum SONR criterion actually benefits from noise. Thus when noise power decreases, this benefit fades and the input SINR drops.

From the above discussions, the following conclusions can be drawn. First, if noise is not considered[2], the three criteria can be seen as equivalent. Second, if noise is considered, the IONR window shows the poorest performance. In fact, it becomes completely useless as will be shown in subsection 5.3.5. Finally, the maximum SONR criterion is advantageous in that it provides a better input SINR when noise is considered.

5.3.3 The Influence of Q

To show the influence of Q, we plot in Fig. 5.3 the input SINR and BAE of the BAE window and the SONR window with respect to different values of Q. The effect of Q is twofold. On the one hand, increasing Q reduces BAE, which is desirable. On the other hand, it also decreases input SINR, which is undesirable. As illustrated in Fig. 5.4, for the minimum BAE criterion, although OOB interference is significantly suppressed when Q is large, in-band interference is unavoidably raised hence causing a reduced

[1] This is similar to pulse shaping in that low-power side lobes and narrow main lobe can not be well achieved at the same time.

[2] This means we don't consider noise in window design in spite of noise power.

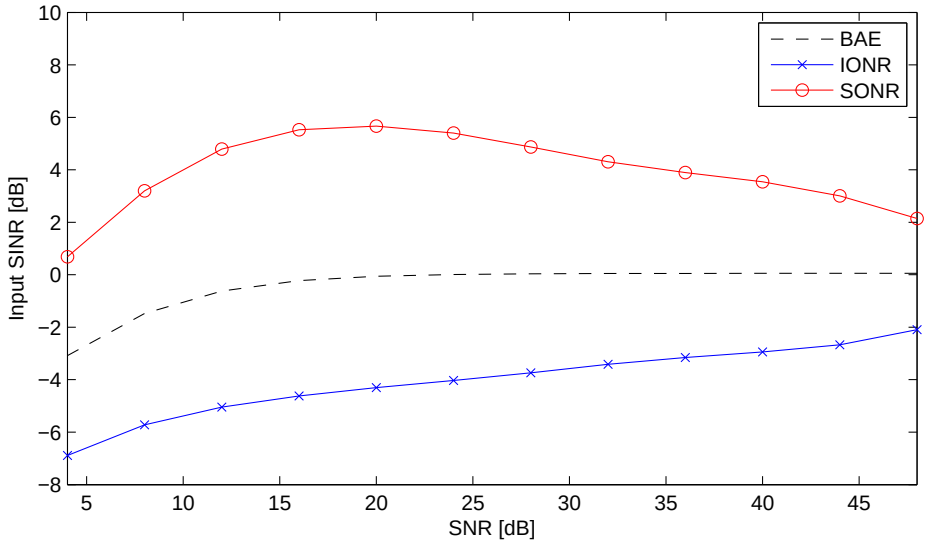

Fig. 5.1: Input SINR comparison of different window design criteria when $Q = 3$.

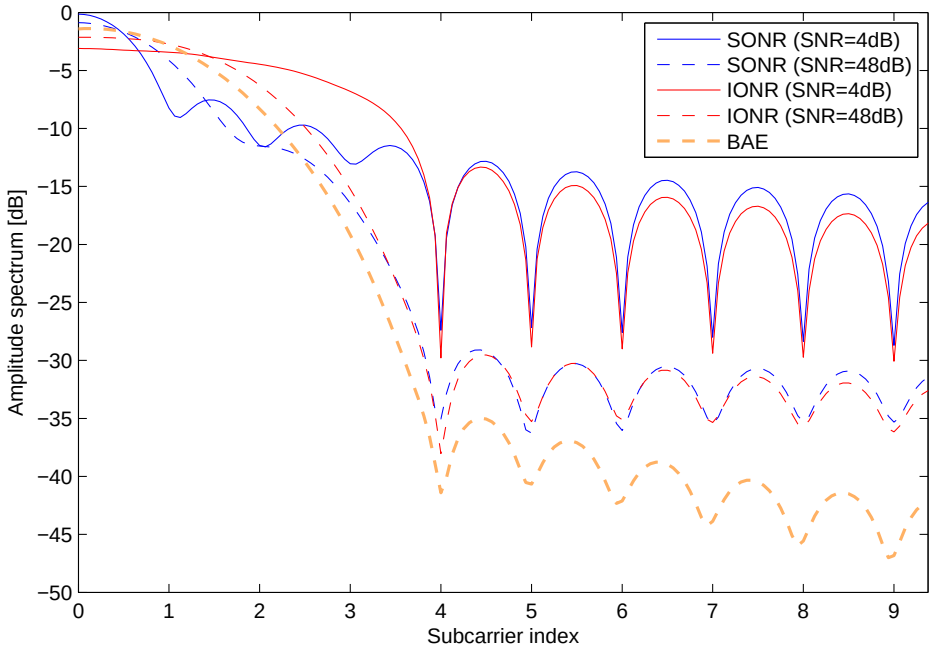

Fig. 5.2: Amplitude spectrum comparison of different window design criteria when $Q = 3$.

input SINR. This effect is less pronounced in the maximum SONR criterion due to its in-band interference suppression capability. However, even so, choosing a large Q is not beneficial in the sense of reducing complexity. Therefore, a simple but effective rule is required for selecting a proper Q.

In this thesis, we propose to evaluate the ratio of OOB interference power to noise

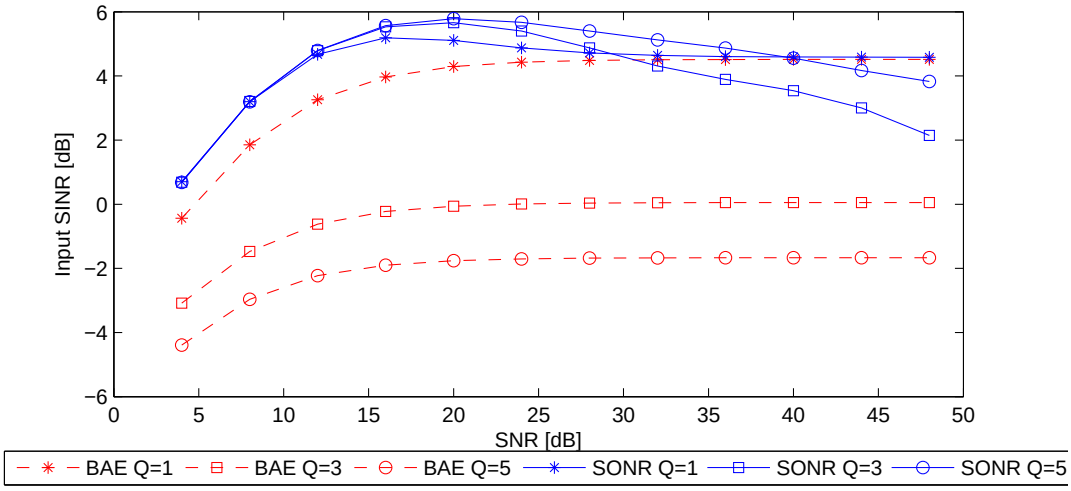

(a) Input SINR

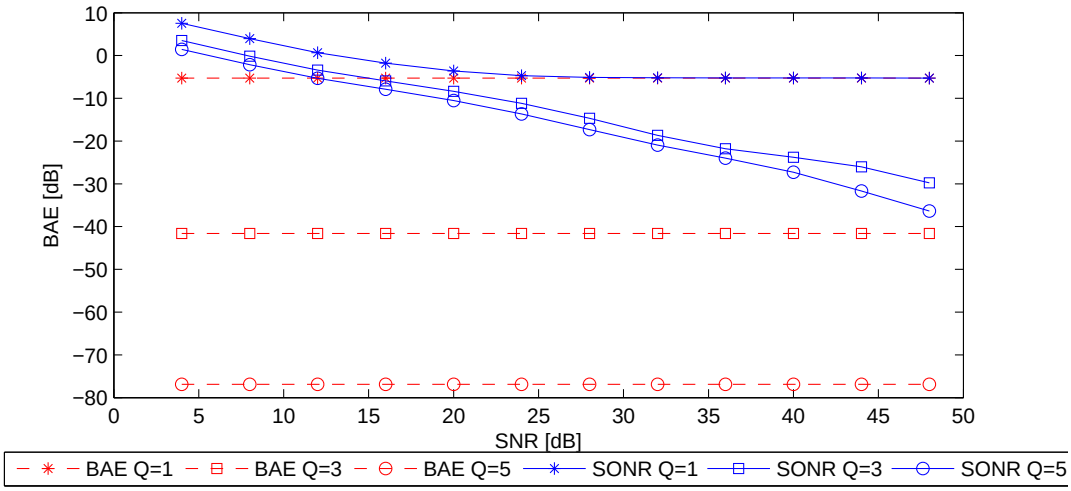

(b) BAE

Fig. 5.3: Input SINR and BAE comparison with respect to Q.

power from $Q = 0$ until $\mathcal{P}_{oob}/\mathcal{P}_n < \mathcal{T}$. A simple choice for $\mathcal{T}$ is one because when $\mathcal{P}_{oob}$ is less than $\mathcal{P}_n$, the influence of OOB interference power is less important than that of noise power. From a better performance point of view, we should use $\mathcal{P}_{oob}/\mathcal{P}_n \ll 1$. However, in this case, the determination of $\mathcal{T}$ requires extensive simulation and field tests. For the channel shown in Fig. 4.3, using $\mathcal{P}_{oob}/\mathcal{P}_n < 1$ gives the result of $Q = 2$. Simulation has shown that $Q = 3$ is a better choice ($Q = 2$ is also good) but $Q = 4$ is not necessary (negligible improvement). To get the result of $Q = 3$, $\mathcal{T}$ should be approximately between 0.06 and 0.2. When channel variation is negligible, this method will give the result of $Q = 0$. This indicates that ICI mitigation is not necessary and the simplest one-tap equaliser can be applied.

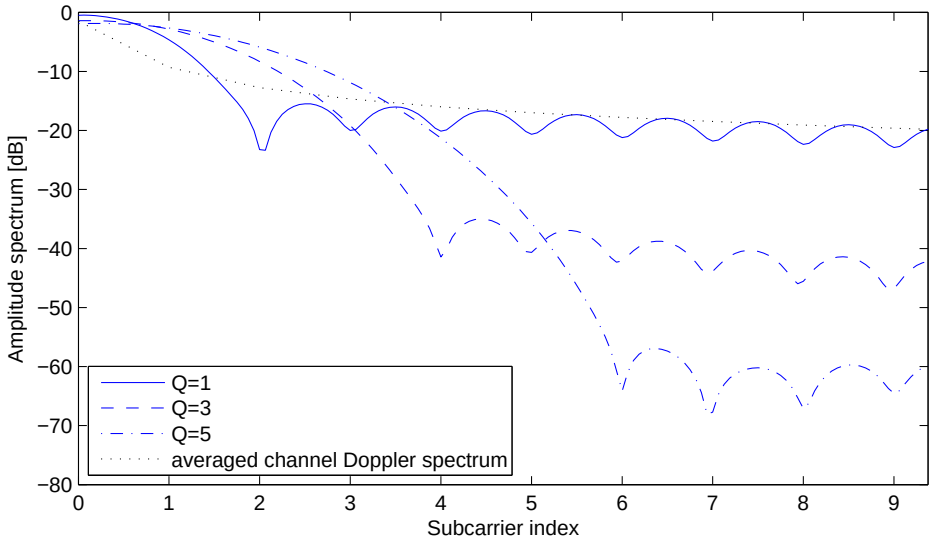

Fig. 5.4: Amplitude spectrum of the windows generated by the minimum BAE criterion with respect to Q.

5.3.4 The SOE Constraint and Complexity Analysis

As stated above, the SOE constraint given in (5.19) ensures that the noise covariance matrix is also banded. The principle behind this constraint is that it performs like a low-pass filter that limits the number of discrete harmonics that comprise the window to $2Q+1$. Simulation has shown that the influence of this limitation to the performance of a window is negligible. On the contrary, it reduces the computational complexity of the eigenvalue decomposition that is required for window design. Originally, eigenvalue decomposition is performed on an $L \times L$ matrix but this is reduced to a $(2Q+1) \times (2Q+1)$ matrix if the SOE constraint is adopted. This process significantly speeds up the determination of window coefficients.

The overall computational complexity of window design is usually not an issue for wireless communication because given the channel statistics, the window can be designed in advance. For time-varying power line channel, this has to be done in real time. Thanks to the periodicity of channel time variation, such a calculation only needs to be done once if the channel topology does not change. However, this requires that OFDM block transmission is synchronous to the mains period, which in turn requires a careful design of OFDM block length.

5.3.5 BER Performance

The output SINR and BER performance using different window design criteria are shown in Fig. 5.5 and Fig. 5.6. These figures are generated when $Q = 3$. From the comparison of output SINR it can seen that the SONR window provides the highest

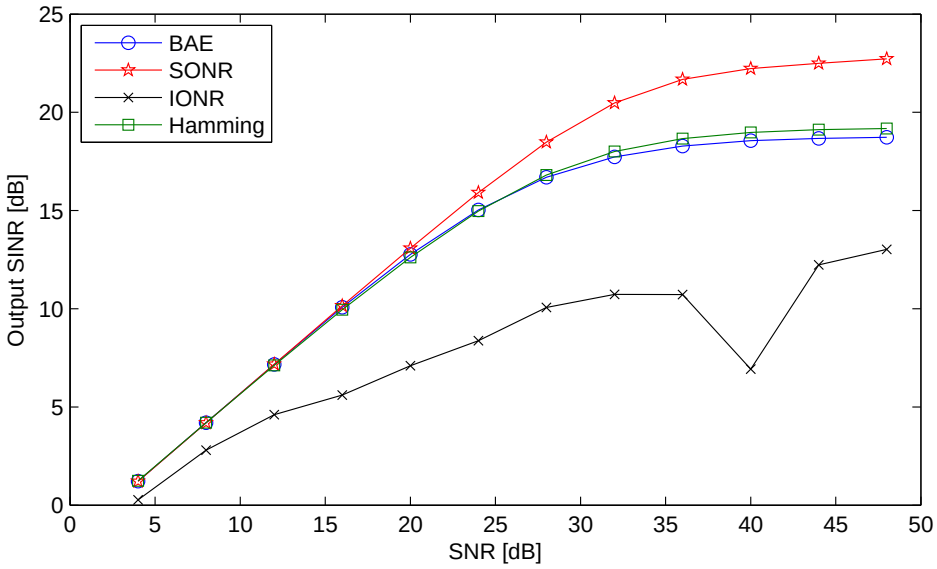

Fig. 5.5: Output SINR comparison of different windows (Q=3).

output SINR. In addition, both the BAE window and the SONR window outperform the banded equaliser without windowing (Fig. 4.4). Note that the performance of the SONR window when $Q = 3$ is even better than the non-window case with $Q = 7$ shown in Fig. 4.4 and Fig. 4.5. On the contrary, the performance of the IONR window is very bad and some strange fluctuation can even be observed. The BER comparison draws the similar conclusions. Particularly, the performance of the SONR windowed MMSE equaliser is very close to the idea conventional MMSE equaliser, whereas the IONR windowed MMSE equaliser sometimes is even worse than the one-tap equaliser. It is known that at high SNR region interference is dominant, hence this shows that the SONR has the best interference suppression ability. In these two figures, the performance of the well-known Hamming window is also included. It can be seen that its performance is close to that of the BAE window but is still not as good as the proposed window design criterion. However, we want to point out that since the implementation of a Hamming window is very simple, if the requirement of performance is not crucial, the Hamming window is a good choice for a low-complexity implementation.

5.4 Summary

In this chapter we presented the algorithms of three window design criteria. With the assistance of simulation, we compared the performance of these criteria. We also discussed the influence of some key parameters in window design.

The following conclusions can be drawn from this study. First, for wireless commu-

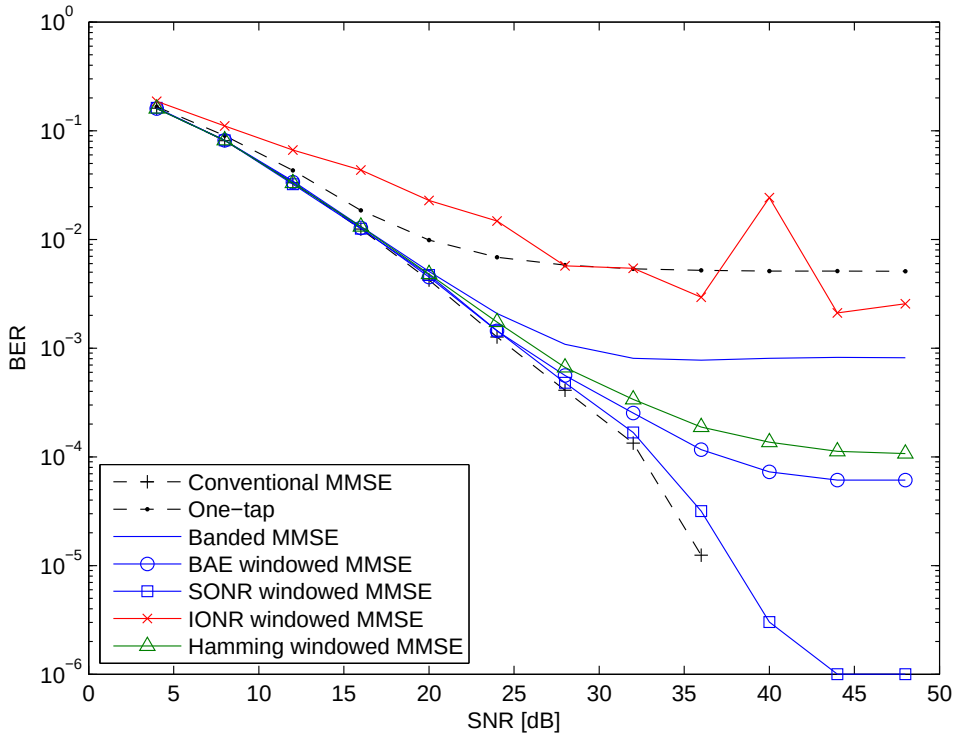

Fig. 5.6: BER comparison of different equalisers (Q=3 for banded equalisers).

nication, these window design criteria present little difference in performance. Among them, the minimum BAE criterion is the simplest but an effective method. Second, for time-varying power line channel, these criteria present similar but limited performance if noise is not considered. For better performance, noise should be considered. However, under this condition, the IONR becomes completely useless. On the contrary, the SONR criterion shows the best performance. Third, a large value of Q may worsen the performance of the minimum BAE criterion but the maximum SONR criterion is more robust to this problem. In order to provide a good balance between complexity and performance, we proposed a simple rule for the determination of Q. Finally, it was found that the SOE constraint not only ensures banded noise covariance matrix but also reduces the computational complexity of window design significantly. Therefore, we recommend to use this constraint for all the window design criteria.

Chapter 6

Conclusion and Future Work

6.1 Conclusion

In this thesis, to aid the development of a low-cost PLC system for smart metering in HANs, power line channel characterisation and modelling were first investigated. After that, a low-complexity banded equaliser with receiver windowing was developed.

6.1.1 Power Line Channel Characterisation and Modelling

In chapter 3 we studied power line channel characterisation and modelling. The power line channel is a very harsh communication media. It is time-varying and frequency-selective, and it presents a strong low-pass behaviour. It is also impaired by a complex impulsive noise scenario.

Power line channel modelling approaches are categorised into top-down approaches and bottom-up approaches. A top-down approach attempts to find the most fitted model from measurements, while in a bottom-up approach the channel model is derived from transmission line theory. Top-down approaches are simple but require massive data collection, and there is no universally accepted models. The bottom-up approaches provide accurate channel realisations but they are hard to be analysed mathematically.

Depending on the cables used in the network, bottom-up approaches are based on either 2TL theory or MTL theory. In this thesis we introduced these theories and developed a flexible simulation tool based on the 2TL theory, the voltage ratio approach [12] and the time-varying channel model proposed in [5]. The simulation tool is used to generate time-varying channel realisations to help verify the developed systems. The key feature of this tool is that it accepts any tree-structured power network topology and a variety of load models. In addition, it can be extended to generating MTL based power line channels.

6.1.2 Banded Equalisation with Receiver Windowing

In chapter 4 we investigated the performance of several linear equalisers for time-varying power line channels and found that the banded equaliser provides a good ICI mitigation

capability while it has a low computational complexity.

To improve the performance of banded equalisers, we investigated receiver windowing in chapter 5. Two well-known window design criteria, namely the minimum BAE criterion and the maximum IONR criterion, were studied. It was found that these two methods do not work well over time-varying power line channels. The minimum BAE criterion proposed in [14] applies a simplification that is not valid over time-varying power line channels. By removing this simplification, this method can be applied to PLC and the performance is quite good. However, the maximum IONR criterion is completely useless for PLC because it enhances in-band interference significantly. In that chapter, we also proposed an alternative window design criterion, called the maximum SONR criterion. Simulations have proved that this criterion outperforms the other two criteria because it provides the highest input and output SINRs.

6.2 Future Work

6.2.1 Power Line Channel Modelling

Since there is no universally accepted power line channel model, channel modelling is still an important and urgent task for PLC system design. A top-down channel model that covers a wide range of PLC applications is of paramount importance. Since top-down models are usually easy-to-analyse, they can be used to help justify the performance of PLC systems mathematically. Extensive measurements are required for important statistical information such as amplitude distribution, power delay profile, RMS delay spread and power spectrum density. In addition, time variation and spatial correlation between end-users are also necessary.

MIMO PLC is another emerging research field that is based on MTLs. However, there is a limited number of research works on the modelling of MIMO channels. Top-down MIMO channel modelling is extremely challenging because it is hard to characterise the coupling between conductors.

6.2.2 Receiver Window Design with Time-Varying Noise

It is assumed that the noise is AWGN in this thesis. However, as mentioned in chapter 3, noise in indoor power network is in fact cyclostationary with time-varying variance. In addition, a variety of impulsive noise should also be expected. Therefore, it is important to consider these noise when designing the window. From the analysis in chapter 5, we can expect that time-varying noise will alter the window but it will not affect too much on window design criteria because interference is the major concern of window design.

Appendix A

Derivation of Mean Squared BAE

The main purpose of this appendix is to show that the derivation of mean squared BAE is different for a wireless channel and a power line channel.

The mean squared BAE is defined as

$$\mathrm{E}[\|\mathbf{E}^{(w)}\|_F^2] = \mathrm{E}[\|\mathbf{H}_F^{(w)}\|_F^2] - \mathrm{E}[\|\mathbf{B}_F^{(w)}\|_F^2] \tag{A.1}$$

where $\mathrm{E}[\|\mathbf{H}_F^{(w)}\|_F^2]$ can be written in quadratic form as

$$\begin{aligned}
\mathrm{E}[\|\mathbf{H}_F^{(w)}\|_F^2] &= \mathrm{E}[\|\mathbf{W}_F\mathbf{H}_F\|_F^2] \\
&= \mathrm{E}[\|\mathbf{W}\mathbf{H}_L\|_F^2] \\
&= \mathrm{E}[\mathrm{tr}\{\mathbf{W}\mathbf{H}_L\mathbf{H}_L^H\mathbf{W}^H\}] \\
&= \mathbf{w}^H\mathcal{D}(\mathrm{E}[\mathcal{H}\mathcal{H}^H])\mathbf{w} \\
&= \mathbf{w}^H\mathcal{D}(\mathbf{R}_{\mathcal{H}\mathcal{H}})\mathbf{w}
\end{aligned} \tag{A.2}$$

where $\mathbf{R}_{\mathcal{H}\mathcal{H}} = \mathrm{E}[\mathcal{H}\mathcal{H}^H]$ and $\mathcal{H}$ are given in (5.7) and (5.8), and explained thereafter.

When the channel is wireless and assuming it is wide-sense stationary uncorrelated scattering (WSSUS) with constant channel energy over time, we have $\mathcal{D}(\mathbf{R}_{\mathcal{H}\mathcal{H}}) = \mathcal{E}_h\mathbf{I}_L$, where $\mathcal{E}_h$ is the energy of channel. Thus, (A.2) becomes $\mathrm{E}[\|\mathbf{H}_F^{(w)}\|_F^2] = \mathcal{E}_h\mathbf{w}^H\mathbf{w} = \mathcal{E}_hL$. It is clear that under this circumstance, $\mathrm{E}[\|\mathbf{H}_F^{(w)}\|_F^2]$ is a constant that does not depend on $\mathbf{w}$. On the contrary, since a time-varying power line channel is deterministic, it has a time-varying channel energy, hence $\mathrm{E}[\|\mathbf{H}_F^{(w)}\|_F^2]$ becomes dependent on $\mathbf{w}$.

The term $\mathrm{E}[\|\mathbf{B}_F^{(w)}\|_F^2]$ is derived as follows (for simplicity, the expectation notation

is omitted)

$$\begin{aligned}
\mathrm{E}[\|\mathbf{B}_F^{(w)}\|_F^2] &= \|\mathbf{T} \circ (\mathbf{W}_F \mathbf{H}_F)\|_F^2 \\
&= \|\mathbf{P}_Q \mathbf{W}_F \mathcal{H}_F\|_F^2 \\
&= \|\mathbf{P}_Q \mathbf{F} \mathbf{W} \mathbf{F}^H \mathbf{F} \mathcal{H} \mathbf{F}\|_F^2 \\
&= \|\mathbf{P}_Q \mathbf{F} \mathbf{W} \mathcal{H}\|_F^2 \\
&= \sum_{l=0}^{L_h-1} \sum_{|k| \le Q} \left| \frac{1}{\sqrt{L}} \sum_{n=0}^{L-1} w_n h_{n,l} \exp\{-j2\pi kn/L\} \right|^2 \\
&= \frac{1}{L} \sum_{n,m,l} w_n w_m^* \sum_{|k| \le Q} \exp\{-j2\pi k(n-m)/L\} h_{n,l} h_{m,l}^* \\
&= \mathbf{w}^H (\mathbf{R}_{\mathcal{H}\mathcal{H}} \circ \mathbf{A}) \mathbf{w} \qquad \text{(A.3)}
\end{aligned}$$

where in order to get rid of the dot product, $\mathbf{T}$ and $\mathbf{H}_F$ are transformed to $\mathbf{P}_Q$ and $\mathcal{H}_F$ respectively. $\mathcal{H}_F$ can be obtained from $\mathbf{H}_F$ by rearranging diagonals as columns, or by $\mathcal{H}_F = \mathbf{F}\mathcal{H}\mathbf{F}$, and

$$\mathbf{P}_Q = \begin{bmatrix} \mathbf{I}_{Q+1} & \mathbf{0} & \mathbf{0} \\ \mathbf{0} & \mathbf{0} & \mathbf{0} \\ \mathbf{0} & \mathbf{0} & \mathbf{I}_Q \end{bmatrix}$$

Finally, for a wireless channel, the mean squared BAE is expressed by

$$\mathrm{E}[\|\mathbf{E}^{(w)}\|_F^2] = \mathcal{E}_h L - \mathbf{w}^H (\mathbf{R}_{\mathcal{H}\mathcal{H}} \circ \mathbf{A}) \mathbf{w} \qquad \text{(A.4)}$$

For a power line channel, it is written as

$$\begin{aligned}
\mathrm{E}[\|\mathbf{E}^{(w)}\|_F^2] &= \mathbf{w}^H \mathcal{D}(\mathbf{R}_{\mathcal{H}\mathcal{H}}) \mathbf{w} - \mathbf{w}^H (\mathbf{R}_{\mathcal{H}\mathcal{H}} \circ \mathbf{A}) \mathbf{w} \\
&= \mathbf{w}^H (\mathbf{R}_{\mathcal{H}\mathcal{H}} \circ (\mathbf{I}_L - \mathbf{A})) \mathbf{w} \qquad \text{(A.5)}
\end{aligned}$$

It should be noted that (A.5) is a general solution that can be used for both power line channels and wireless channels, but (A.4) can only be used for wireless channels.

Appendix B

Derivation of IONR and SONR

In this appendix, we show the derivation of IONR and SONR. The IONR is originally derived in [13], and we derive the SONR accordingly. In order to use the generalised eigenvalue problem to find the desired optimal solution, they are expressed in quadratic forms.

The simplest way to derive IONR is to derive the in-band signal power $\mathcal{P}_{ib}$ and the total received signal power $\mathcal{P}_t$, and use (5.13). The in-band signal power has been derived in (A.3) as $\mathcal{P}_{ib} = \mathrm{E}[\|\mathbf{B}_F^{(w)}\|_F^2] = \mathbf{w}^H(\mathbf{R}_{\mathcal{H}\mathcal{H}} \circ \mathbf{A})\mathbf{w}$. Here we derive the total received signal power, as given by

$$\begin{aligned}
\mathcal{P}_t &= \mathcal{P}_{ib} + \mathcal{P}_{oob} + \mathcal{P}_n \\
&= \mathrm{E}[\|\mathbf{y}^{(w)}\|_F^2] \\
&= \mathrm{E}[\|\mathbf{W}\mathbf{x}\|_F^2] \\
&= \sum_{n,m} w_n w_m^* \mathrm{tr}\{\mathrm{E}[\mathbf{x}\mathbf{x}^H]\} \\
&= \mathbf{w}^H \mathcal{D}(\mathrm{E}[\mathbf{x}\mathbf{x}^H])\mathbf{w} \\
&= \mathbf{w}^H \mathcal{D}(\mathbf{R}_{\mathcal{H}\mathcal{H}} + \sigma^2 \mathbf{I}_L)\mathbf{w}
\end{aligned} \tag{B.1}$$

As a result, the IONR is given by

$$\mathrm{IONR}(\mathbf{w}) = \frac{\mathcal{P}_{ib}}{\mathcal{P}_t - \mathcal{P}_{ib}} = \frac{\mathbf{w}^H(\mathbf{R}_{\mathcal{H}\mathcal{H}} \circ \mathbf{A})\mathbf{w}}{\mathbf{w}^H(\mathcal{D}(\mathbf{R}_{\mathcal{H}\mathcal{H}} + \sigma^2\mathbf{I}_L) - \mathbf{R}_{\mathcal{H}\mathcal{H}} \circ \mathbf{A})\mathbf{w}} \tag{B.2}$$

Now we derive the SONR in a similar way. The *useful signal* power $\mathcal{P}_s$ can be obtained by letting $Q = 0$ in (A.3), as expressed by

$$\begin{aligned}
\mathcal{P}_s &= \|\mathcal{D}(\mathbf{W}_F\mathbf{H}_F)\|_F^2 \\
&= \|\mathbf{P}_0\mathbf{F}\mathbf{W}\mathcal{H}\|_F^2 \\
&= \frac{1}{L}\sum_{n,m,l} w_n w_m^* h_{n,l} h_{m,l}^* \\
&= \frac{1}{L}\mathbf{w}^H \mathbf{R}_{\mathcal{H}\mathcal{H}}\mathbf{w}
\end{aligned} \tag{B.3}$$

Then it is straightforward to get SONR as

$$\mathrm{SONR}(\mathbf{w}) = \frac{\mathcal{P}_s}{\mathcal{P}_t - \mathcal{P}_{ib}} = \frac{\mathbf{w}^H(\mathbf{R}_{\mathcal{H}\mathcal{H}}/L)\mathbf{w}}{\mathbf{w}^H(\mathcal{D}(\mathbf{R}_{\mathcal{H}\mathcal{H}} + \sigma^2\mathbf{I}_L) - \mathbf{R}_{\mathcal{H}\mathcal{H}} \circ \mathbf{A})\mathbf{w}} \tag{B.4}$$

To obtain the window coefficients that maximise IONR and SONR, we use the generalised eigenvalue problem as shown in (5.14) and (5.17).

Finally, similar to the minimum BAE criterion, (B.2) and (B.4) can be simplified when we consider a wireless channel with constant channel energy. That is

$$\mathrm{IONR}(\mathbf{w}) = \frac{\mathbf{w}^H(\mathbf{R}_{\mathcal{H}\mathcal{H}} \circ \mathbf{A})\mathbf{w}}{\mathbf{w}^H((\mathcal{E}_h + \sigma^2)\mathbf{I}_L - \mathbf{R}_{\mathcal{H}\mathcal{H}} \circ \mathbf{A})\mathbf{w}} \tag{B.5}$$

$$\mathrm{SONR}(\mathbf{w}) = \frac{\mathbf{w}^H(\mathbf{R}_{\mathcal{H}\mathcal{H}}/L)\mathbf{w}}{\mathbf{w}^H((\mathcal{E}_h + \sigma^2)\mathbf{I}_L - \mathbf{R}_{\mathcal{H}\mathcal{H}} \circ \mathbf{A})\mathbf{w}} \tag{B.6}$$

Bibliography

[1] M. Nassar, J. Lin, Y. Mortazavi, A. Dabak, I. Kim, and B. Evans, "Local Utility Power Line Communications in the 3500 kHz Band: Channel Impairments, Noise, and Standards," *IEEE Signal Processing Magazine*, vol. 29, no. 5, pp. 116–127, Sep. 2012.

[2] P. Amirshahi, F. Cañete, K. Dostert, S. Galli, M. Katayama, and M. Kavehrad, *Power Line Communications: Theory and Applications for Narrowband and Broadband Communications over Power Lines*, 1st ed. New York: Wiley, 2010, ch. Channel Characterization.

[3] M. Babic, M. Hagenau, K. Dostert, and J. Bausch, "Theoretical postulation of plc channel models," the OPERA IST Integrated Project, Tech. Rep., 2005.

[4] C. Paul, *Analysis of Multiconductor Transmission Lines*, 2nd ed. New Jersey: John Wiley and Sons, 2008.

[5] F. Canete, J. Cortes, L. Diez, and J. Entrambasaguas, "A channel model proposal for indoor power line communications," *IEEE Communications Magazine*, vol. 49, no. 12, pp. 166–174, Dec. 2011.

[6] M. Katayama, T. Yamazato, and H. Okada, "A mathematical model of noise in narrowband power line communication systems," *IEEE Journal on Selected Areas in Communications*, vol. 24, no. 7, pp. 1267–1276, Jul. 2006.

[7] X. Fang, S. Misra, G. Xue, and D. Yang, "Smart grid - the new and improved power grid: A survey," *Communications Surveys Tutorials, IEEE*, vol. 14, no. 4, pp. 944–980, Apr. 2012.

[8] S. Galli, A. Scaglione, and Z. Wang, "For the Grid and Through the Grid: The Role of Power Line Communications in the Smart Grid," *Proceedings of the IEEE*, vol. 99, no. 6, pp. 998–1027, Jun. 2011.

[9] F. Corripio, J. Arrabal, L. del Rio, and J. Munoz, "Analysis of the cyclic short-term variation of indoor power line channels," *IEEE Journal on Selected Areas in Communications*, vol. 24, no. 7, pp. 1327–1338, Jul. 2006.

[10] J. Cortés, L. Díez, F. Cañete, J. Sánchez-Martínez, and J. Entrambasaguas, "Performance analysis of OFDM modulation on indoor broadband PLC channels," *EURASIP Journal on Advances in Signal Processing*, vol. 2011, no. 1, p. 78, 2011.

[11] W. Zhu, X. Zhu, E. G. Lim, and Y. Huang, "State-of-art power line communications channel modelling," *Procedia Computer Science*, vol. 17, no. 0, pp. 563 – 570, 2013.

[12] A. M. Tonello and F. Versolatto, "Bottom-Up Statistical PLC Channel Modeling-Part I: Random Topology Model and Efficient Transfer Function Computation," *IEEE Transactions on Power Delivery*, vol. 26, no. 2, pp. 891–898, Apr. 2011.

[13] P. Schniter, "Low-Complexity Equalization of OFDM in Doubly Selective Channels," *IEEE Transactions on Signal Processing*, vol. 52, no. 4, pp. 1002–1011, Apr. 2004.

[14] L. Rugini, P. Banelli, and G. Leus, "Low-Complexity Banded Equalizers for OFDM Systems in Doppler Spread Channels," *EURASIP Journal on Advances in Signal Processing*, vol. 2006, pp. 1–14, 2006.

[15] Z. M. Fadlullah, M. M. Fouda, N. Kato, A. Takeuchi, N. Iwasaki, and Y. Nozaki, "Toward intelligent machine-to-machine communications in smart grid," *IEEE Communications Magazine*, Apr. 2011.

[16] A. Ghassemi, S. Bavarian, and L. Lampe, "Cognitive radio for smart grid communications," in *IEEE International Conference on Smart Grid Communications*, 2010.

[17] D. Niyato, L. Xiao, and P. Wang, "Machine-to-machine communications for home energy management system in smart grid," *IEEE Communications Magazine*, Apr. 2011.

[18] R. P. Lewis, P. Igic, and Z. Zhou, "Assessment of communication methods for smart electricity metering in the u.k." in *IEEE PES/IAS Conference on Sustainable Alternative Energy*, 2009.

[19] G. N. Srinivasa Prasanna, A. Lakshmi, S. Sumanth, V. Simha, and G. Bapat, J. abd Koomullil, "Data communication over the smart grid," in *IEEE International Symposium on Power Line Communications and Its Applications*, 2009.

[20] J. Liu, B. Zhao, L. Geng, Z. Yuan, and Y. Wang, "Communication performance of broadband plc technologies for smart grid," in *IEEE International Symposium on Power Line Communications and Its Applications*, 2011.

[21] F. Hlawatsch and G. Matz, Eds., *Wireless Communications Over Rapidly Time-Varying Channels*. Oxford, UK: Elsevier, 2011.

[22] S. Galli, "A Novel Approach to the Statistical Modeling of Wireline Channels," *IEEE Transactions on Communications*, vol. 59, no. 5, pp. 1332–1345, May 2011.

[23] M. Zimmermann and K. Dostert, "A multipath model for the powerline channel," *IEEE Transactions on Communications*, vol. 50, no. 4, pp. 553–559, Apr. 2002.

[24] S. Guzelgoz, H. B. Celebi, and H. Arslan, "Statistical Characterization of the Paths in Multipath PLC Channels," *IEEE Transactions on Power Delivery*, vol. 26, no. 1, pp. 181–187, Jan. 2011.

[25] A. M. Tonello, F. Versolatto, B. Bejar, and S. Zazo, "A Fitting Algorithm for Random Modeling the PLC Channel," *IEEE Transactions on Power Delivery*, vol. 27, no. 3, pp. 1477–1484, Jul. 2012.

[26] M. Tlich, A. Zeddam, F. Moulin, and F. Gauthier, "Indoor Power-Line Communications Channel Characterization Up to 100 MHzPart I: One-Parameter Deterministic Model," *IEEE Transactions on Power Delivery*, vol. 23, no. 3, pp. 1392–1401, Jul. 2008.

[27] A. M. Tonello and F. Versolatto, "Bottom-Up Statistical PLC Channel Modeling-Part II: Inferring the Statistics," *IEEE Transactions on Power Delivery*, vol. 25, no. 4, pp. 2356–2363, Oct. 2010.

[28] S. Galli and T. Banwell, "A deterministic frequency-domain model for the indoor power line transfer function," *IEEE Journal on Selected Areas in Communications*, vol. 24, no. 7, pp. 1304–1316, Jul. 2006.

[29] ——, "A Novel Approach to the Modeling of the Indoor Power Line ChannelPart II: Transfer Function and Its Properties," *IEEE Transactions on Power Delivery*, vol. 20, no. 3, pp. 1869–1878, Jul. 2005.

[30] T. Banwell and S. Galli, "A Novel Approach to the Modeling of the Indoor Power Line Channel Part I: Circuit Analysis and Companion Model," *IEEE Transactions on Power Delivery*, vol. 20, no. 2, pp. 655–663, Apr. 2005.

[31] T. Esmailian, F. R. Kschischang, and P. Glenn Gulak, "In-building power lines as high-speed communication channels: channel characterization and a test channel ensemble," *International Journal of Communication Systems*, vol. 16, no. 5, pp. 381–400, Jun. 2003.

[32] D. Anastasiadou and T. Antonakopoulos, "Multipath Characterization of Indoor Power-Line Networks," *IEEE Transactions on Power Delivery*, vol. 20, no. 1, pp. 90–99, Jan. 2005.

[33] F. Versolatto and A. M. Tonello, "An MTL Theory Approach for the Simulation of MIMO Power-Line Communication Channels," *IEEE Transactions on Power Delivery*, vol. 26, no. 3, pp. 1710–1717, Jul. 2011.

[34] T. Sartenaer and P. Delogne, "Deterministic modeling of the (shielded) outdoor power line channel based on the multiconductor transmission line equations," *IEEE Journal on Selected Areas in Communications*, vol. 24, no. 7, pp. 1277–1291, Jul. 2006.

[35] H. Meng, S. Chen, Y. Guan, C. Law, P. So, E. Gunawan, and T. Lie, "Modeling of Transfer Characteristics for the Broadband Power Line Communication Channel," *IEEE Transactions on Power Delivery*, vol. 19, no. 3, pp. 1057–1064, Jul. 2004.

[36] E. G. Bakhoum, "S-Parameters Model for Data Communications Over 3-Phase Transmission Lines," *IEEE Transactions on Smart Grid*, vol. 2, no. 4, pp. 615–623, Dec. 2011.

[37] G. Marrocco, D. Statovci, and S. Trautmann, "A PLC broadband channel simulator for indoor communications," in *2013 IEEE 17th International Symposium on Power Line Communications and Its Applications*. IEEE, Mar. 2013, pp. 321–326.

[38] A. Tomasoni, R. Riva, and S. Bellini, "Spatial correlation analysis and model for in-home MIMO power line channels," in *2012 IEEE International Symposium on Power Line Communications and Its Applications*. IEEE, Mar. 2012, pp. 286–291.

[39] N. Rao, *Elements of Engineering Electromagnetics*, 6th ed. New Jersey: Pearson Prentice Hall, 2004.

[40] D. Cheng, *Fundamentals of Engineering Electromagnetics*. New Jersey: Pearson Prentice Hall, 1993.

[41] H. Meng, Y. L. Guan, and S. Chen, "Modeling and Analysis of Noise Effects on Broadband Power-Line Communications," *IEEE Transactions on Power Delivery*, vol. 20, no. 2, pp. 630–637, Apr. 2005.

[42] M. Zimmermann and K. Dostert, "Analysis and modeling of impulsive noise in broad-band powerline communications," *IEEE Transactions on Electromagnetic Compatibility*, vol. 44, no. 1, pp. 249–258, 2002.

[43] D. Benyoucef, "A new statistical model of the noise power density spectrum for powerline communication," in *2003 IEEE International Symposium on Power Line Communications and Its Applications*, 2003.

[44] D. Middleton, "Statistical-physical models of electro-magnetic interference," *IEEE Transactions on Electromagnetic Compatibility*, vol. EMC-19, no. 3, pp. 106 – 127, Aug. 1977.

[45] R. S. Blum, Y. Zhang, B. M. Sadler, and R. J. Kozick, "On the approximation of correlated non-gaussian noise pdfs using gaussian mixture models," in *Proceedings of the 1st Conference on the Applications of Heavy Tailed Distributions in Economics, Engineering and Statistics*, 1999.

[46] L. Rugini, P. Banelli, and G. Leus, "Simple equalization of time-varying channels for OFDM," *IEEE Communications Letters*, vol. 9, no. 7, pp. 619–621, Jul. 2005.

[47] G. H. Golub and C. F. V. Loan, *Matrix Computations*, 3rd ed. Baltimore, London: The Johns Hopkins University Press, 1996.

[48] W. C. Jakes, *Microwave Mobile Communications*, 2nd ed. New York: Wiley, 1994.